



Contents lists available at ScienceDirect

Environmental Pollution

journal homepage: www.elsevier.com/locate/envpol

Contrasting temporal dynamics of dissolved and colloidal trace metals in the Pearl River Estuary

Minwei Xie ^{a, b}, Wen-Xiong Wang ^{b, c, *}^a College of the Environment and Ecology, Xiamen University, Fujian, 361102, China^b Research Centre for the Oceans and Human Health, City University of Hong Kong Shenzhen Research Institute, Shenzhen, 518057, China^c School of Energy and Environment, State Key Laboratory of Marine Pollution, City University of Hong Kong, Kowloon, Hong Kong, PR China

ARTICLE INFO

Article history:

Received 5 February 2020

Received in revised form

25 May 2020

Accepted 2 June 2020

Available online 7 June 2020

Keywords:

Behavior of trace metal

Estuarine mixing

Spatial and temporal variability

Colloids

Hydrology

Biogeochemical process

ABSTRACT

Metal contamination in the Pearl River Estuary (PRE) is persistent-, yet a comprehensive understanding of distribution and behavior of metals in surface water of this large, multi-source estuary is still lacking. In the present study, water samples from 24 sites spanning the whole estuary during the dry and wet season were collected and fractionated. Trace metal concentrations in samples were then determined following a preconcentration technique using Nobias Chelate-PA1 resin. Distribution of trace metals exhibited variability along and across estuary, as a result of estuarine mixing, external metal loadings, addition and removal. Behavior of metals was contrasting between the dry and wet seasons, exhibiting metal-specific intercorrelations and dynamics. Colloidal metals (Mn, Ni and Cd) were primarily present in upper estuary and areas affected by external contaminant loading. Colloidal Cu was the only metal that was ubiquitous in the estuary in both seasons. It showed a high affinity for small-size organic colloids (likely fulvic acid) during the dry season. Overall, the present study demonstrated the multi-source character of the PRE and that the behavior of trace metals was controlled by the coupling of hydrologic and geochemical processes, with anthropogenic perturbations.

© 2020 Elsevier Ltd. All rights reserved.

1. Introduction

The Pearl River Estuary (PRE), the second largest estuary in China, is surrounded by several megacities on its fringe. Decades of rapid economic development in these cities have released excessive chemicals into the estuary and caused environmental issues (Dai et al., 2008; Li et al., 2000; Wang et al., 2014). Among these issues, metal contamination is persistent: enrichment of Cu, Pb and Zn in the estuarine sediments were dated back to 1970s, when urbanization and industrialization in this region initiated (Ip et al., 2004); a more recent survey in 2011 covering the same sampling sites revealed no alleviation in contamination over the past decade (Chen et al., 2012). Though metal concentration profiles in sediment documented a history of metal contamination in the estuary, the ecological effects of metal contamination have only been investigated recently.

Systematic investigations demonstrated that the ecological

impacts of metal contamination in the PRE showed spatiotemporal variability. Fang et al. (2003) observed enrichment of multiple metals in oysters along both coasts of the estuary, with oysters accumulated much higher concentrations along western coast relative to eastern coast. But contamination hotspots on eastern coast have emerged more recently (Chan and Wang, 2019b; Yin and Wang, 2017; Yu et al., 2013). As a result of continuous metal exposure, adverse outcomes shifted oysters' population structure: over a year-round investigation, Weng and Wang (2019) for the first time reported significant changes in the reproductive cycle and an imbalance of sex ratios of oyster population at contaminated sites compared with a reference site, which was likely due to the endocrine-disrupting effects of metals. Clearly, the ecological impacts of metal contamination on local aquatic organisms depend on metals loading, and are further complicated by metals behavior within the estuary.

Surprisingly, there has been limited work on behavior of trace metals in the PRE waters, possibly due to the late start of scientific investigations in Asian estuaries (including the PRE) (Chen et al., 2004). Within the estuary, dissolved metal concentrations was determined sparsely at a few sites (Wang et al., 2012; Yin and

* Corresponding author. School of Energy and Environment, State Key Laboratory of Marine Pollution, City University of Hong Kong, Kowloon, Hong Kong
E-mail address: wx.wang@cityu.edu.hk (W.-X. Wang).

Wang, 2017), whereas a comprehensive understanding of metal behavior is still lacking. Given that the hydrographic and geochemical conditions between estuaries are distinct, barely a universal pattern can depict the behavior of trace metals in different estuaries (Hatje et al., 2003). This circumstance is even more complex in the PRE, due to its spatially multi-source character—receiving water loadings from multiple tributaries and contaminants from different sources—and seasonally distinct circulation dynamics (Brigden et al., 2009; Chen et al., 2004; Wang et al., 2012). Therefore, a better understanding of metal behavior in the PRE waters is essential to assessing the relevant environmental impacts.

Accordingly, the primary objective of the present study was to advance the understanding of how the interplay of hydrological and geochemical processes within the estuary controls behavior of trace metals and influences their spatial and temporal distributions. To achieve this, surface water samples from sites spanning the whole estuary were fractionated by filtration and ultrafiltration, and analyzed for trace metal concentrations; and behavior of trace metals were inferred based on the spatial distribution and temporal variation of metal concentrations in the PRE.

2. Material and methods

2.1. Study site

The PRE is a complex estuarine system receiving water from an interlaced upstream river network (Pearl River network) (Hu et al., 2011). To the north of the estuary, riverine flow from different sources enters the estuary through four main outlets—HuMen, JiaoMen, Hongqili and HengMen (Fig. 1). Flow scouring and suspended particle deposition, together with waterway dredging, shaped the estuary topography into three shoals (with water depth shallower than 5 m) and two deep channels (the West and East

Channel, 5–15 m in depth) (Zhang et al., 2019). Based on the geomorphology and hydrology characteristics, the PRE is divided into three sections (Fig. 1) (Wang et al., 2012): the upper estuary is characterized by a deep—and—narrow channel and receives longitudinal flow primarily from the HuMen; the middle estuary consists of two shallow shoals and one deep channel, and the lateral flow from the HengMen and Hongqili outlets converges with the longitudinal flow into the estuary; the lower estuary consists of two wide shoals and two channels and the water is predominantly controlled by the estuarine mixing.

Seasonal variations in the hydrographic conditions are pronounced in the PRE due to strong precipitation in the wet season. Annually, the funnel-shaped estuary discharges more than 60% of the freshwater runoff from the upper Pearl River drainage basin (Zhang et al., 2019). Eighty percent of the annual flow occurred in the wet season between April and September (Xia et al., 2004). During the wet season, high riverine flow dominates the surface water; denser seawater intrudes into the estuary as a salt wedge in the bottom layer, leading to vertical stratification in the estuary (Wong et al., 2003). In contrast, in the dry season, because of the low river discharge, seawater intrusion extends further upstream into the Pearl River, resulting in slight stratification near HuMen outlet but water in the remaining part of the estuary is vertically homogeneous (Harrison et al., 2008).

2.2. Sampling and processing of water samples

Collection of surface water in the PRE was conducted in March and August of 2017, representing the dry and wet seasons respectively. The dry season sampling survey started 1 h before the high tide and finished 1 h past the low tide (8 h in total, the tidal range is 0.9 m); the wet season sampling survey was conducted on two consecutive days, each started at the low tide and finished about 1 h before the high tide (tidal ranges were 0.6 and 0.5 m).

Prior to sample collection, all plasticware was cleaned by soaking in 10% HNO₃ (puriss grade, Sigma-Aldrich) for 24 h and by rinsing thoroughly with deionized water. Twenty-four sites spanning the whole estuary were selected, including 3 sites located at the river outlet (HuMen, JiaoMen, and the confluence of flow from Hongqili and HengMen—referred to as HengMen) and 21 sites along the western, central and eastern transects (W-, C- and E-transects) (Fig. 1). At each site, 1.5 L of surface water was collected by hand-submersion of a polypropylene bottle beneath the water surface. Meanwhile, salinity, dissolved oxygen (DO) concentration and pH of the water were measured on board with a YSI probe (YSI Pro Plus). Once the sampling survey was finished, water samples were transported to laboratory for further processing.

To obtain metal concentrations in different fractions—total dissolved (<0.4 μm), truly dissolved (<1 kDa) and colloidal (1 kDa–0.4 μm) fractions, water samples were either filtered or ultrafiltered using filters with different pore sizes. Using 0.4 μm polycarbonate membrane filter (Millipore), low-vacuum filtration of all water samples was accomplished within 24 h following the sample collection. Concentrations of metals in the filtrate are referred as total dissolved metal concentrations ([Mn]_{0.4μm}, [Ni]_{0.4μm}, [Cu]_{0.4μm}, [Zn]_{0.4μm}, and [Cd]_{0.4μm}). An aliquot of the filtrate (~400 mL) was further ultrafiltered using a 400-mL stirred cell ultrafiltration unit (Amicon) equipped with a 1 kDa regenerated cellulose membrane disc. Metals in the permeate solution are referred as truly dissolved metals. The filtrate and ultrafiltered permeate solutions were acidified to pH ~2 with HCl (Optima®, Thermo Fisher Scientific, Inc.), and stored at 4 °C until preconcentration and determination of trace metals. Dissolved organic matter (DOM) properties in the filtrate, ultrafiltered permeate solution and retained colloidal material were also characterized using a spectrofluorometer and an

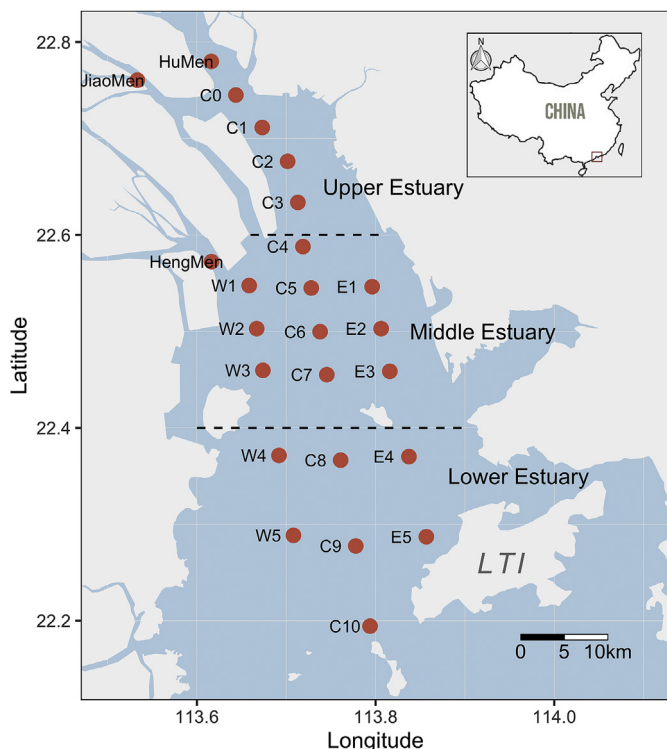


Fig. 1. Location of the Pearl River Estuary and sampling sites.

asymmetric flow-field flow fractionation instrument, and reported in a companion study (Xie et al., 2018). Readers may refer to our prior publication for further details of the dynamics of DOM in the estuary (Xie et al., 2018).

2.3. Preconcentration and analysis of water samples

Both filtered and ultrafiltered estuarine water samples were preconcentrated using Nobias Chelate-PA1 resin (Hitachi High-Technologies) following procedures described in Sorhin et al. (2008) before determination of metal concentrations. To prevent inadvertent contamination, the preconcentration of water samples was conducted in an all-plastic laminar flow clean bench (Class-100). Prior to use, the new resin was extensively cleaned according to the procedures described by Sorhin et al. (2008) and was then packed into pre-cleaned polypropylene columns (6 mm inner diameter, 1 cm bed height) and sandwiched between two porous polyethylene frits. Concentrated acetic acid–ammonium acetate buffer (3.6 M, pH = 6.0, herein referred to as concentrated buffer) was also prepared and purified by passing twice through a Nobias Chelate-PA1 column and diluted to 0.05 M when necessary (herein referred to as diluted buffer). To process six samples simultaneously, we used a manifold of 6 resin columns connected to a peristaltic pump. Before loading of samples, the columns were cleaned with 20 mL of 1 M HNO₃ (puriss grade, Sigma-Aldrich), flushed with 30 mL of deionized water, and conditioned with 40 mL of diluted buffer at a constant flow rate of 3 mL/min. To the acidified water samples (260 g, pH=2) was added 3.65 g of concentrated buffer, achieving a final concentration of 0.05 M, and the pH was adjusted to 6.0 by adding ammonia or HCl. The buffered water samples were then loaded onto the resin columns at a flow rate of 3 mL/min, followed by 40 mL of diluted buffer to flush sea salts remaining in the columns. The target metals bound to the resin were finally eluted with 10 mL of 1 M HNO₃ (Optima®, Thermo Fisher Scientific, Inc.) at a flow rate of 1 mL/min into test tubes (Falcon, Corning) before analysis.

2.4. Quality control and metal analysis

To test the recovery and reproducibility of the preconcentration operation, a series of saline reference samples were processed by the same preconcentration procedures. These samples included a 50-mL NASS-6 reference seawater sample (National Research Council of Canada, NRCC), a 50-mL SLEW-3 estuarine water sample (NRCC), and several liters of filtered natural seawater (collected from NanAo, Shenzhen) spiked with known amount of target metals. To test whether filtration, ultrafiltration or preconcentration caused inadvertent contamination, procedural blank samples were also prepared by processing deionized water with the same operation protocols, and determined as unknown water samples.

Metal concentrations in the eluate were determined using an inductively coupled plasma mass spectrometer (ICP-MS, Agilent 7800) for Mn, Ni, Cu, Zn, and Cd. ⁷²Ge and ¹¹⁵In were used as internal standards to correct the instrument drift. Certified reference river water SLRS-6 (NRCC) was also subjected to the same analytical procedures and was repeatedly measured after every 30 samples.

Preconcentration of metals from saline water samples using Nobias chelate PA-1 resin was robust, providing high recovery (90–115%) and reproducibility (<10% relative standard deviation) and inducing minimal contamination (Supporting Information). Filtration did not contaminate water samples. Ultrafiltration also did not cause contamination of Mn, Ni, Cu and Cd, but induced Zn contamination in the procedural blank (Table S2). Therefore, truly dissolved Zn concentrations and colloidal Zn concentrations are not presented.

2.5. Statistical analysis

Statistics were carried out in RStudio (v1.2.5019). Principal component analysis (PCA) was performed to evaluate correlations between metals within the whole estuary, and to study the spatial variabilities in metal distributions. PCA was accomplished using the “prcomp” function, with the variance of each variable standardized to unit before analysis. Correlations between metals and organic components were conducted using “cor” function, while partial correlation analysis with the effect of salinity controlled was achieved using “pcor” function in the “ggm” package.

3. Results and discussions

3.1. Physicochemical parameters

The salinity, DO concentrations, and pH of water samples at all sites during both the dry and wet seasons are shown in Table S2, Supporting information. Surface water in the PRE was saltier in the dry season than in the wet season: salinity increased seaward from 0.22 at the head of the estuary to 30.5 at the mouth of the estuary during the dry season; in contrast, salinity was much lower during the wet season, increasing seaward from 0.13 to 15.0 (Xie et al., 2018).

Distribution of DO concentrations in surface water also exhibited strong spatial and temporal variabilities (Table S2, Fig. S4). In both seasons, surface water from the HuMen outlet was relatively depleted in DO concentrations (<4.0 mg/L, <50% saturation). The low-oxygen plume from the HuMen outlet advected downstream and mixed with oxygenated water in the estuary, increasing the DO concentrations back to the oxygenated level (>6.5 mg/L). During the dry season, the low-DO plume extended for ~15 km from HuMen to site C2 (DO = 6.8 mg/L, 79% saturation) along the C-transect. Surface water in the remaining sites of C-transect, as well as sites in the W- and E-transect were well oxygenated (>7.0 mg/L, >80% saturation). In contrast, during the wet season, the low-oxygen plume extended further to site C4 (~25 km, DO = 6.3 mg/L, 85% saturation) along the C-transect. A low-oxygen zone was also observed along the E-transect from site E1 to E4 where DO slightly decreased from 4.8 to 3.5 mg/L (49–65% saturation). Surface water in the W-transect and other sites in the C-transect remained oxygenated (>6.3 mg/L, >85% saturation).

Distribution of pH was spatially uniform during the dry season (pH = 8.0 ± 0.2); in contrast, during the wet season, distribution of pH showed a similar pattern as that of DO. Along the C-transect, pH gradually increased from 6.7 at the HuMen outlet to 8.2 at site C5 and remained at 8.2 toward the mouth of the estuary. Also in sites along the E transect, pH was slightly lower (8.0 ± 0.1) relative to that at the sites of the same latitude along the C-transect (C5–C9, pH = 8.3 ± 0.1) and W-transect (W1–W5, pH = 8.2 ± 0.1).

3.2. Distribution of the total dissolved metals in the estuary

Total dissolved metal concentrations of surface water were in the range of 4.1–1200 nM for Mn, 9.2–150 nM for Ni, 7.5–35 nM for Cu, 1.8–75 nM for Zn, and 0.14–0.99 nM for Cd respectively. These values were at comparable levels with those reported in prior studies of PRE (Wang et al., 2012; Yin and Wang, 2017). Overall, [Mn]_{0.4μm}, [Ni]_{0.4μm}, and [Zn]_{0.4μm} in the dry season were higher relative to those in the wet season (paired *t*-test, *p* < 0.01 for Mn and Ni; *p* < 0.05 for Zn), whereas [Cu]_{0.4μm} and [Cd]_{0.4μm} were at similar concentration range during both sampling seasons (*p* > 0.05) (Figs. 2 and 3).

Metal distributions showed spatial variability along and across the estuary during the dry season. Along the C-transect, all metal

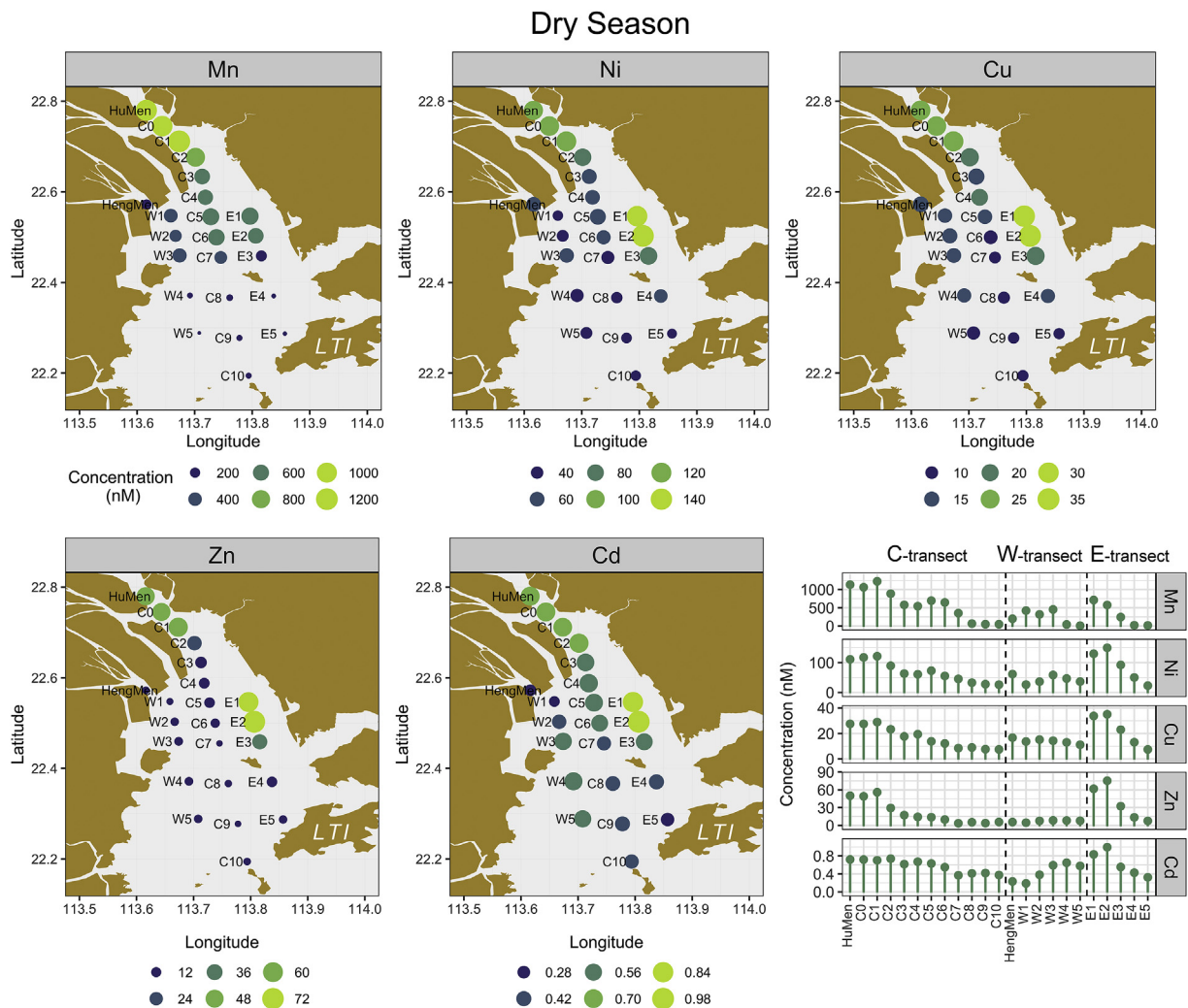


Fig. 2. Distribution of total dissolved metals during the dry season.

concentrations consistently decreased (Fig. 2), suggesting that flow through HuMen outlet may represent a major source of these metals into the estuary. In the middle estuary, distribution of metals deviated between different transects (Figs. 2 and 4): $[\text{Ni}]_{0.4\mu\text{m}}$, $[\text{Cu}]_{0.4\mu\text{m}}$, $[\text{Zn}]_{0.4\mu\text{m}}$, and $[\text{Cd}]_{0.4\mu\text{m}}$ at sites E1 and E2 along the E-transect were much higher than those at sites in the same latitude (C5 and C6) along the C-transect; in contrast, all metals at sites HengMen, W1 and W2 along the W-transect were much lower relative to C5 and C6. In the lower estuary, metal concentrations were at comparable levels between different transects.

Spatial variability in metal distributions was also observed during the wet season, but metal-specific: different metals showed distinct distribution (Fig. 3). Along the C-transect, $[\text{Ni}]_{0.4\mu\text{m}}$, $[\text{Cu}]_{0.4\mu\text{m}}$ and $[\text{Zn}]_{0.4\mu\text{m}}$ decreased rapidly in the region with salinity < 2.5 and remained at low levels as the salinity exceeded 2.5 (Fig. 4); in contrast, $[\text{Mn}]_{0.4\mu\text{m}}$ and $[\text{Cd}]_{0.4\mu\text{m}}$ increased seaward to a concentration maximum in the lower salinity region (salinity < 7), followed by a slight decrease as salinity exceeded 12 (Fig. 4). Similar to the dry season, metal distributions also deviated in the middle estuary during the wet season: metal concentrations were higher along the E transect (site E1 and E2) but lower in the W transect (site HengMen, W1 and W2) relative to those at sites in the C transect (C5, C6) (Fig. 3). However, the magnitude of the concentration differences between transects in the wet season was

much lower than that in the dry season (Figs. 2 and 3). In the lower estuary, except $[\text{Mn}]_{0.4\mu\text{m}}$ and $[\text{Ni}]_{0.4\mu\text{m}}$ that still exhibited transect differences, $[\text{Cu}]_{0.4\mu\text{m}}$, $[\text{Zn}]_{0.4\mu\text{m}}$, and $[\text{Cd}]_{0.4\mu\text{m}}$ were uniform between transects.

The spatial and temporal variability in metal distributions was further interpreted using PCA. Here, PCA reduced data into two dimensions while retaining maximal information: 86.6% and 82.2% of the total variance in the dataset during the dry and wet season (Fig. 5). Based on their loading scores, metals were divided into two groups in both seasons. During the dry season, a group of Cu, Ni, Zn and Cd was clustered in the top left quadrant (Fig. 5a), indicating their high correlations; the other group consisting solely of Mn vector was nearly perpendicular to vectors in the former group (Fig. 5a), suggesting Mn distribution within the estuary was not correlated with other metals. During the wet season, a group consisting of Cu, Zn and Ni had high negative scores on the first principle component, while the other group consisting of Mn and Cd clustered into the bottom right quadrant (Fig. 5b).

The spreading of sites in the PCA biplot reflected the spatial variability of metal distributions within the estuary. Projection of sites onto a metal vector indicated their relative metal concentration levels.

Metal distributions in the dry season were characterized with an evident concentration gradient from upper to lower estuary, and

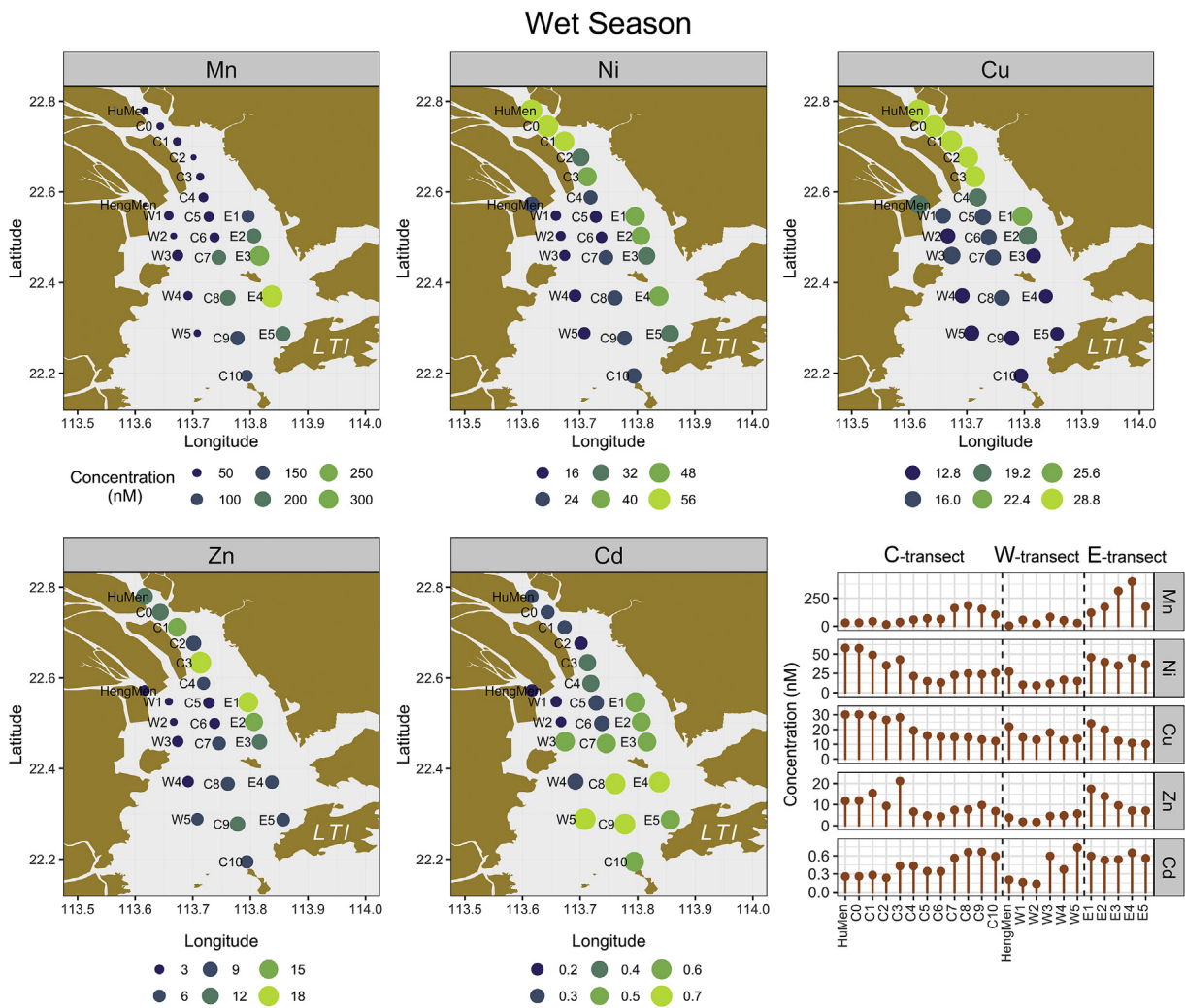


Fig. 3. Distribution of total dissolved metals during the wet season.

with a concentration hotspot (site E2) contributing to cross-estuary heterogeneity (Fig. 5a): sites in the upper estuary and lower estuary were compactly clustered, and located diagonally from high metal-concentration end to low metal-concentration end; sites in the middle estuary, except those along the E-transect, were located between the two clusters. Site E2, with the highest rank on projections to the Cu, Ni, Zn, and Cd vectors, represented a hotspot of these four metals in the estuary.

During the wet season, the spatial variability in metal distribution were metal specific (Fig. 5b): concentration gradients of Cu, Ni and Zn were primarily along estuary; in contrast, concentration gradients of Mn and Cd were both along estuary (from lower to upper estuary) and across estuary (from E- to W-transect).

3.3. Dynamics of metals along the C-transect

Away from the western and eastern coasts of the PRE, the external input of metals is of lesser importance along the C-transect, which makes it an ideal transect for assessing fate and behavior of metals under estuarine mixing processes. Estuarine mixing has a conservative index—salinity; and thus a conservative behavior of a constituent often corresponds to a linear relationship between constituent concentrations and salinity in the mixing diagram (Day et al., 1989).

The mixing diagrams of total dissolved metal concentrations along salinity in the C-transect during the dry and wet seasons are shown in Fig. 4. As mentioned previously, metal concentrations decreased with increasing salinity in the dry season, meaning mixing with seawater was an important mechanism driving the decline in metal concentrations. Distributions of $[Mn]_{0.4\mu m}$, $[Ni]_{0.4\mu m}$, $[Cu]_{0.4\mu m}$, $[Zn]_{0.4\mu m}$ with salinity were below the theoretical mixing lines (Fig. 4), suggesting nonconservative behavior of these metals and certain removal processes scavenged these metals. In contrast, $[Cd]_{0.4\mu m}$ declined linearly with the salinity during the dry season ($r = -0.936$, $p < 0.01$) (Fig. 4), indicating the conservative behavior of Cd during mixing in the salinity range of 7–30.

During the wet season, the distribution of $[Ni]_{0.4\mu m}$, $[Cu]_{0.4\mu m}$, $[Zn]_{0.4\mu m}$ along salinity gradient declined rapidly in the lower salinity region (salinity < 2.5) and then remained about constant (Fig. 4), resulting in concave distributions of Ni, Cu and Zn along the C-transect and suggesting the nonconservative behavior of these three metals. The distribution of Mn and Cd also showed nonconservative features, but with an increase in concentrations in the lower salinity region (salinity < 7) and a subsequent decline in higher salinity range (salinity > 12), suggesting addition of these two metals into the dissolved pool.

The common trends in metal concentrations along salinity

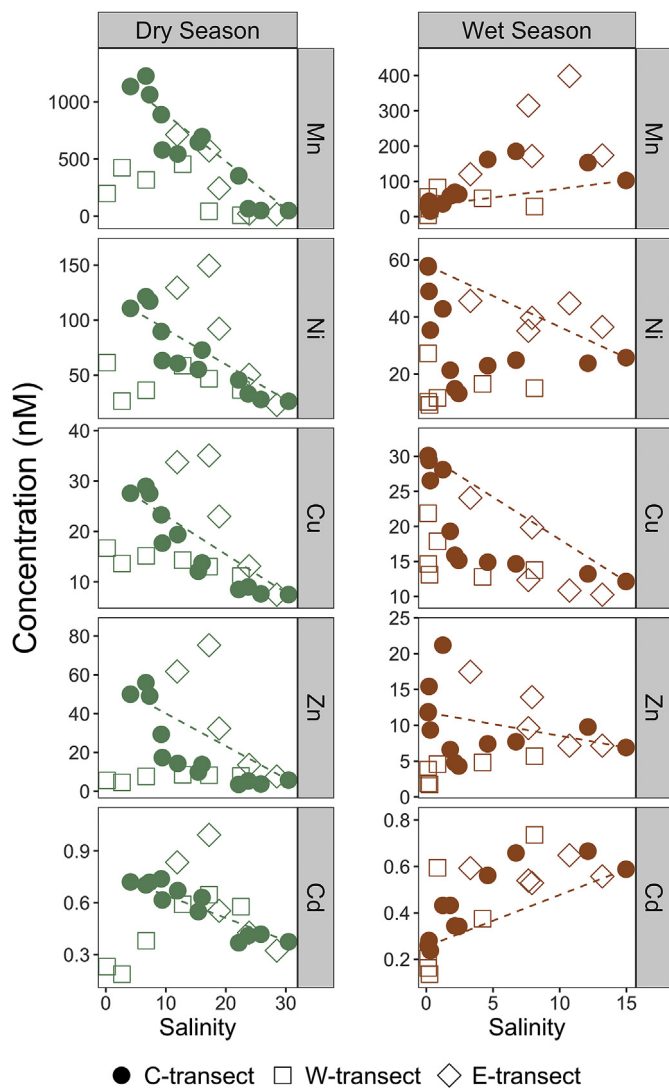


Fig. 4. Distribution of total dissolved metal concentrations along the salinity gradient in both the dry and wet season. Dashed lines indicate the theoretical conservative mixing lines along the C-transect.

gradient often inform potential association and common behavior between metals over the course of estuarine mixing. Discerning the association of them directly based on their correlations is however problematic, particularly when they span a large salinity range. Variables that do not have true correlation, may end up correlated because they each correlate with salinity. To exclude this artifact, we performed pairwise partial correlation analysis on metal concentrations by controlling for the effect of salinity. The result was compared with direct pairwise correlation analysis to discern the true correlations between metals, and to discriminate the relative importance of physical (estuarine dilution) and geochemical processes (removal/addition) in controlling the distribution of metals (Fig. 6).

Besides intercorrelations between metals, correlations between dissolved organic matter (DOM) and metals was also evaluated, as DOM is an important complexation ligand for trace metals (Bianchi, 2007; van den Berg et al., 1987). DOM was represented by four fluorescent components, which were adopted from a companion study sharing the same sampling sites (Xie et al., 2018). The DOM fluorescent components (EEM_C1 to _C4) were derived from a parallel factor analysis of the excitation and emission matrices of

filtered water samples. Briefly, these components represent microbially derived humic-like component (C1), tryptophan-like component (C2), terrestrial humic-like component (C3), and tyrosine-like component (C4), respectively.

Correlation patterns were different between the dry and wet season (Fig. 6a and b). During the dry season, the scatter plots showed strong, positive, linear correlations between the concentrations of all metals and the fluorescent intensity of DOM components ($p < 0.01$) (Fig. S1, Fig. 6a). In contrast, during the wet season, correlation patterns were diverse (Fig. S2, Fig. 6b): $[Mn]_{0.4\mu m}$ was positively correlated with $[Cd]_{0.4\mu m}$, but both inversely correlated with $[Cu]_{0.4\mu m}$ and all DOM components; $[Ni]_{0.4\mu m}$, $[Cu]_{0.4\mu m}$ and $[Zn]_{0.4\mu m}$ were positively correlated. Cu was the only metal in the wet season that strongly correlated with all the four DOM components ($p < 0.01$), indicating its high affinity for DOM (Stumm and Morgan, 2012). Relatively weaker correlations between metals and DOM were observed for $[Ni]_{0.4\mu m}$, but not observed for $[Zn]_{0.4\mu m}$.

During the dry season, the broad features of partial correlation results were similar to the correlation results (Fig. 6c and d). Mn, Ni, Cu and Zn were mostly intercorrelated with each other and correlated to at least one DOM component. This suggested that these four metals shared similar removal processes during the estuarine mixing, and were likely associated along the C-transect. Cd was the only metal that did not correlate with either other metals or any DOM components, suggesting that estuarine mixing effect controlled its distribution during the dry season.

During the wet season, partial correlation results revealed that Ni, Cu, Zn, and the four DOM components were significantly intercorrelated ($p < 0.05$) (Fig. 6d). These correlations suggest these three metals experienced similar removal processes and were likely associated. The likely association of Mn and Cd along the C-transect was also supported by their high correlations (Fig. 6d), which also suggests they shared similar addition processes into the dissolved metal pool. By excluding the effects of estuarine mixing, the results clearly indicated similarity in the geochemical behavior within the Ni, Cu and Zn pairs, and within the Mn and Cd pairs along the C-transect during the wet season.

3.4. Multi-source metal loadings to the estuary

The upper estuary receives water primarily from the upstream Pearl River network. DOM in the Pearl River showed similar spectroscopic composition as that in the estuary, and was identified a primary source of DOM into the estuary (Xie et al., 2018). The high correlation between fluorescent intensity of DOM components and metal concentrations along the C-transect implied common source between the two (Fig. 6), suggesting riverine source for all metals during the dry season and Ni, Cu, and Zn in the wet season. This hypothesis was further supported by higher metal concentrations reported in the upstream rivers, as a result of intensive perturbations from anthropogenic activities, such as municipal and industrial sewage discharge, mining (Brigden et al., 2009; Dai et al., 2008; Meng et al., 2013; Wang et al., 2012). Therefore, loading from upstream Pearl River network was a primary source of metals into the upper estuary.

The middle estuary showed cross-estuary variability in metal distribution, highlighting the multi-source character of metal loading. Flow through the HengMen outlet was depleted in metals compared with that through the HuMen outlet (Table S3), leading to much lower metal concentrations at sites adjacent to the HengMen outlet along the W-transect (Figs. 2 and 3). In contrast, higher metal concentrations observed at sites E1 and E2, due to their proximity to the local industrial areas on the eastern coast of the estuary. These contamination hotspots were in agreement with

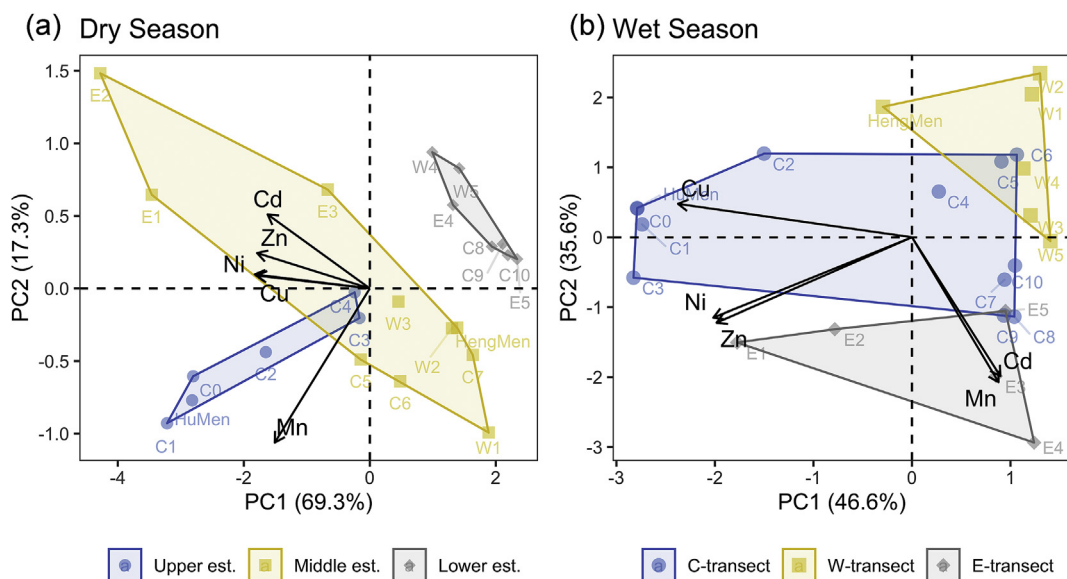


Fig. 5. PCA of metal concentrations illustrated the spatial and temporal variability of metals in the PRE.

other studies, which observed higher metal concentrations in water, oysters and sediments in this region (Chan and Wang, 2019b; Ma et al., 2020; Xie et al., 2019; Yin and Wang, 2017; Yu et al., 2013).

While the multi-source metal loadings in the middle estuary caused variability in metal concentrations, their impacts were relatively localized: the spatial variability was rapidly eliminated by intensive estuarine mixing with water transport to downstream, resulting in a uniform distribution of metal concentrations in the lower estuary (Figs. 2 and 3).

3.5. Temporal variability in the distribution of dissolved Cd and Mn

Distribution of $[Cd]_{0.4\mu m}$ and $[Mn]_{0.4\mu m}$ was distinct between the dry and wet seasons (Fig. 4). In the dry season, distribution of $[Cd]_{0.4\mu m}$ behaved conservatively while $[Mn]_{0.4\mu m}$ exhibited a nonconservative removal along the C-transect. In contrast, during the wet season, distribution of $[Cd]_{0.4\mu m}$ and $[Mn]_{0.4\mu m}$ was significantly correlated and showed a nonconservative addition.

Desorption of Cd from suspended particulates likely explained the nonconservative addition of Cd into the dissolved pool. Release of Cd from suspended particulates was promoted by increasing salinity, as a result of Cd-chloro complexes formation and decreasing free Cd^{2+} activity (Comans and van Dijk, 1988). This salinity promoted desorption process tended to occur in the low salinity region (with salinity < 6–12), and was also frequently reported in many other studies (Bianchi, 2007; Comans and van Dijk, 1988; Kraepiel et al., 1997; Yang and Sañudo-Wilhelmy, 1998).

In the present study, we observed that $[Cd]_{0.4\mu m}$ increased in low salinity region (salinity < 7) but decreased when salinity exceeded 12 along the C-transect during the wet season (Fig. 4). In contrast, particulate Cd concentrations decreased with increasing salinity along the C-transect (Fig. S3a). Except a few sites (HuMen, C1 and C5), free Cd^{2+} activity was strongly correlated with the particulate Cd concentrations, following a linear sorption isotherm model (Fig. S3c). This trend suggested that equilibrium was reached at most sites along the C-transect within the water residence time, and more importantly, the desorption of Cd was regulated by decreasing Cd^{2+} activity along the salinity gradient. Further, we compared the net gains of Cd into the dissolved fraction and net loss of Cd from the particulate fraction, and estimated that

desorption-liberated Cd was responsible for the majority of Cd ($88 \pm 5\%$) mobilized into the aqueous solution (Fig. S3b).

Although $[Cd]_{0.4\mu m}$ and $[Mn]_{0.4\mu m}$ along the C-transect showed significant correlation (Fig. 6d), they were not correlated when all three transects were considered as a whole ($p = 0.255$, partial correlation analysis controlled for salinity), suggesting that their overall behavior within the estuary may be different. The difference was clearly illustrated by their distributions within the estuary: a clear hotspot existed in the estuary for dissolved Mn (site E4), but not for dissolved Cd (Fig. 3).

Based on the current dataset, we were not able to resolve the underlying mechanism of the distribution of dissolved Mn. But we proposed a hypothesis to explain its distribution: benthic release of dissolved Mn, as a result of diagenesis, contributed to the formation of a concentration hotspot in surface water; current circulation within the estuary transported dissolved Mn along and across the estuary, shaping into the observed distribution.

Water stratification became prevalent in the PRE during the wet season, as a combined result of high seaward discharge in surface flow and landward intrusion of bottom seawater (Dai et al., 2008; Wong et al., 2003; Zhang et al., 2019). Continuous DO consumption in bottom seawater along with limited water renewal depleted DO in benthic layer (Dyer, 1991). DO-deficient zones in bottom water frequently developed during the wet season in lower PRE (Qian et al., 2018), favoring reductive dissolution of Mn-oxide minerals. Dissolved Mn was then enriched in the low-oxygen bottom water. Subsequently, the Mn-enriched bottom water may be advected by turbulent mixing and/or upwelling events across the halocline, forming a dissolved Mn hotspot in surface water (Fig. S5) (Dyer, 1991; Harrison et al., 2008; Qian et al., 2018).

In the PRE, saltwater intrusion mainly occurred through two deep channels: the west channel (coincides with the C-transect), and the east channel (as indicated on Fig. S4) (Zhang et al., 2019). Upward entrainment of low-oxygen and Mn-rich bottom water may occur near site E4 during sample collection. Under a typical counter clockwise current circulation in the wet season (Harrison et al., 2008), dissolved Mn in the surface water was transported both along and across estuary, shaping into the observed distribution of dissolved Mn (Fig. S4).

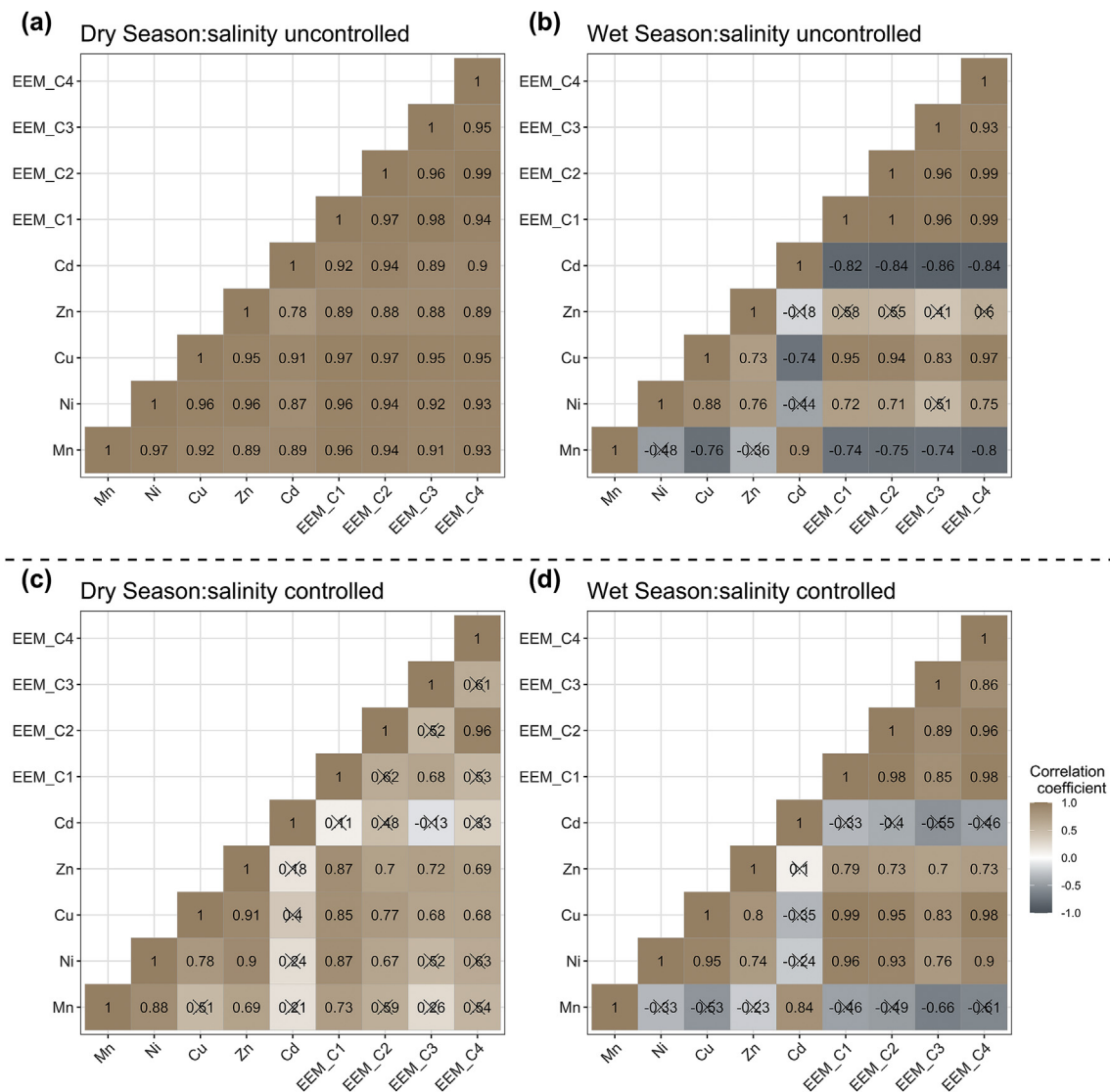


Fig. 6. Pairwise correlation (a, b) and partial pairwise correlation (c, d) between metal concentrations and fluorescent intensities of DOM components (EEM_C1 to C4) along the C-transect during both the dry and wet season. The numbers in each cell represent the Pearson correlation coefficient between each pair. Crossed-off cells indicate the pairs that were not significantly correlated ($p > 0.05$). The fluorescent intensity of DOM components (EEM_C1 to C4) were adapted from Xie et al. (2018).

3.6. Distribution of colloidal metals in the estuary

The general features in distributions of truly dissolved metal concentrations (<1 kDa) were similar to those of total dissolved metals (Figs. S6 and S7). More than 80% of total dissolved Mn, Ni and Cd were in truly dissolved fraction whereas 60–70% for Cu (Fig. S8), suggesting that dissolved Mn, Ni and Cd consisted primarily of low molecular weight species (<1 kDa) but a significant fraction of dissolved Cu were in colloidal forms (1 kDa–0.4 μm).

The difference between the total dissolved and truly dissolved fraction of metals was interpreted as colloidal metal concentrations. The distribution of colloidal Mn, Ni and Cd was scattered, mainly present in upper estuary and sites affected by external contaminant sources (Fig. 7). It is worth noting that at sites along the E-transect, colloidal metal concentrations were consistently high during the dry season and declined seaward (Fig. 7), suggesting that a major fraction of metals discharged from the contaminant source was in the form of colloids. But these colloids were rapidly removed when water mass propagated seaward. In contrast, such features were absent during the wet season, likely as

a result of high flushing rates of surface water that substantially diluted the external pollution. Unlike the other three metals, colloidal Cu was ubiquitous across the whole estuary during both the dry and wet season (Fig. 7).

3.7. Association between colloidal Cu and colloidal organic matter

Given that colloidal Cu represented a significant fraction of total dissolved Cu (30–40%) and was ubiquitous across the estuary, it is important to understand the partitioning of colloidal Cu in the estuary. Accordingly, we evaluated the true correlations between colloidal Cu and organic colloids by performing partial correlation analysis with salinity controlled. The partial correlation coefficients and significance levels are reported in Tables S5–S7.

In the companion study, we investigated the composition and properties of colloidal organic matter using an asymmetric flow field-flow fractionation technique (Xie et al., 2018). This chromatography-like technique generated continuous absorbance and fluorescence spectra over the colloidal size fraction (1.2–400 nm) and provided concentrations of three type of organic

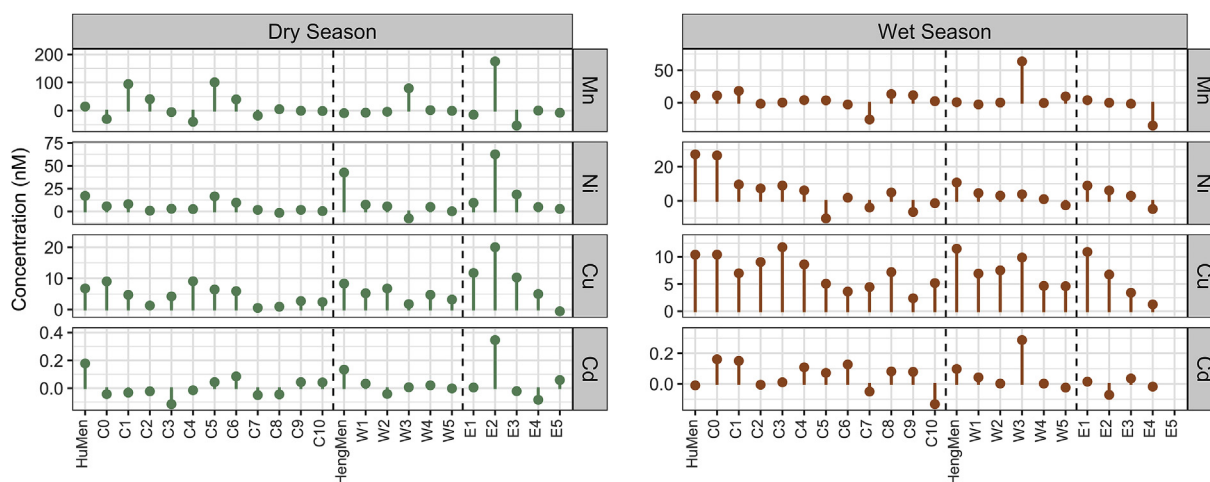


Fig. 7. Distribution of colloidal metals in the PRE.

colloids (chromophoric, humic-type and protein-type) at three size fractions: 1.2–4 nm, 4–24 nm and 24–400 nm.

True correlations between Cu and organic colloids occurred in the dry season but not in the wet season (Figs. 8 and S9). During the dry season, significant correlations were found in the small size fraction (1.2–4 nm): colloidal Cu was significantly correlated with chromophoric, humic-type, and protein-type colloids in the C- and E-transects ($p < 0.01$). This finding was congruent with prior studies that also evidenced higher affinity of colloidal Cu to organic colloids of similar spectroscopic and size properties (Stolpe et al., 2010; Wang et al., 2017). Such organic colloids were identified as natural fulvic acid (Stolpe et al., 2010). Therefore, during the dry season, fulvic acid may function as a binding agent for colloidal Cu.

Concentration ratios of Cu to organic colloids were different between different transects (Fig. 8). Slopes of the regression lines were 3 times higher of the E-transect relative to those of the C-transect for both chromophoric and humic-type organic colloids, indicating that fulvic acid enriched more Cu at E-transect sites because of the external loading of Cu.

During the wet season, true correlations between colloidal Cu and the three type of organic colloids were absent (Fig. S9, Tables S5–S7), suggesting the complexity of binding between Cu and organic colloids. Organic matter in aquatic environment has heterogeneous compositions, including fluorescent and non-fluorescent components, both of which were effective binding agents for Cu (Xu et al., 2014). Further, organic matter with different properties transforms in low salinity region (salinity < 5) (i.e. converting non-fluorescent organic matter to fluorescent products) (Callahan et al., 2004). With a much shorter water residence time during the wet season (< 1 day) (Dupra et al., 2000), such complexities may result in abrupt changes in association between Cu and organic colloids. In contrast, during the dry season, longer water residence time within the estuary (~ 5 days) (He et al., 2010) may favor the equilibration between Cu and organic colloids, yielding association between the two.

3.8. Implications in assessment of metal contamination in the PRE

Biomonitoring of metal contamination in the PRE using local bivalve species started more than two decades ago (Chan and Wang, 2019b; Fang et al., 2003; Weng and Wang, 2019; Yin and Wang, 2017; Yu et al., 2013). Some of the findings from the present study can be used to explain the biomonitoring results. Hot spots of metal contaminations (Cu, Zn and Ni) in oysters were

frequently reported at sites along the eastern coast (near E1 and E2) (Chan and Wang, 2019b; Yin and Wang, 2017). Here, we also observed a hotspot of dissolved and colloidal metals in sites E1 and E2, and attributed it to the adjacency to the industrial areas on the eastern coast. The coincidence of high metal concentrations in different environmental media provided a strong evidence for metal pollution, and thus suggested management efforts such as controlling contaminant sources are needed to mitigate the pollution effects in this region.

Although dissolved Cd concentrations were similar between sites E1–E2 and W3–W4, oyster from sites W3–W4 had higher tissue Cd concentrations than those at sites E1–E2 (Chan and Wang, 2019b; Yin and Wang, 2017). The inconsistency may be explained by the effect of salinity, dietary contribution (uptake from suspended particles) or a combination of both: discharge of riverine flow lowered salinity in sites W3–W4 relative to sites E1–E2 (Table S1), favoring Cd uptake from the estuarine water (Tan et al., 2019); desorption of Cd also tended to occur in low salinity region (Comans and van Dijk, 1988). Together, Cd bioavailability in water and suspended particles at sites W3–W4 were higher than that at sites E1–E2.

4. Conclusions

The present study investigated the distribution and behavior of dissolved and colloidal metals in the PRE and demonstrated:

- Metal distributions in the PRE showed strong spatial variability: in the dry season, metal distributions were featured with a concentration gradient along estuary, and a concentration hotspot on the E-transect; in the wet season, the spatial variability was metal specific—concentration gradients for Cu, Ni and Zn were along estuary while gradients for Mn and Cd were both along and across estuary.
- Estuarine mixing controlled the distribution of dissolved metals in the estuary; meanwhile, removal and addition processes also induced anomalies in the distribution.
- During the dry season, Mn, Ni, Zn, and Cu were highly inter-correlated along the C-transect, but behavior of Cd was independent; in contrast, during the wet season, Ni, Zn and Cu were inter-correlated while Mn and Cd were correlated.
- Colloidal metals (Mn, Ni, and Cd) were primarily present in upper estuary and regions affected by external metal loadings. Colloidal Cu was ubiquitous across the whole estuary.

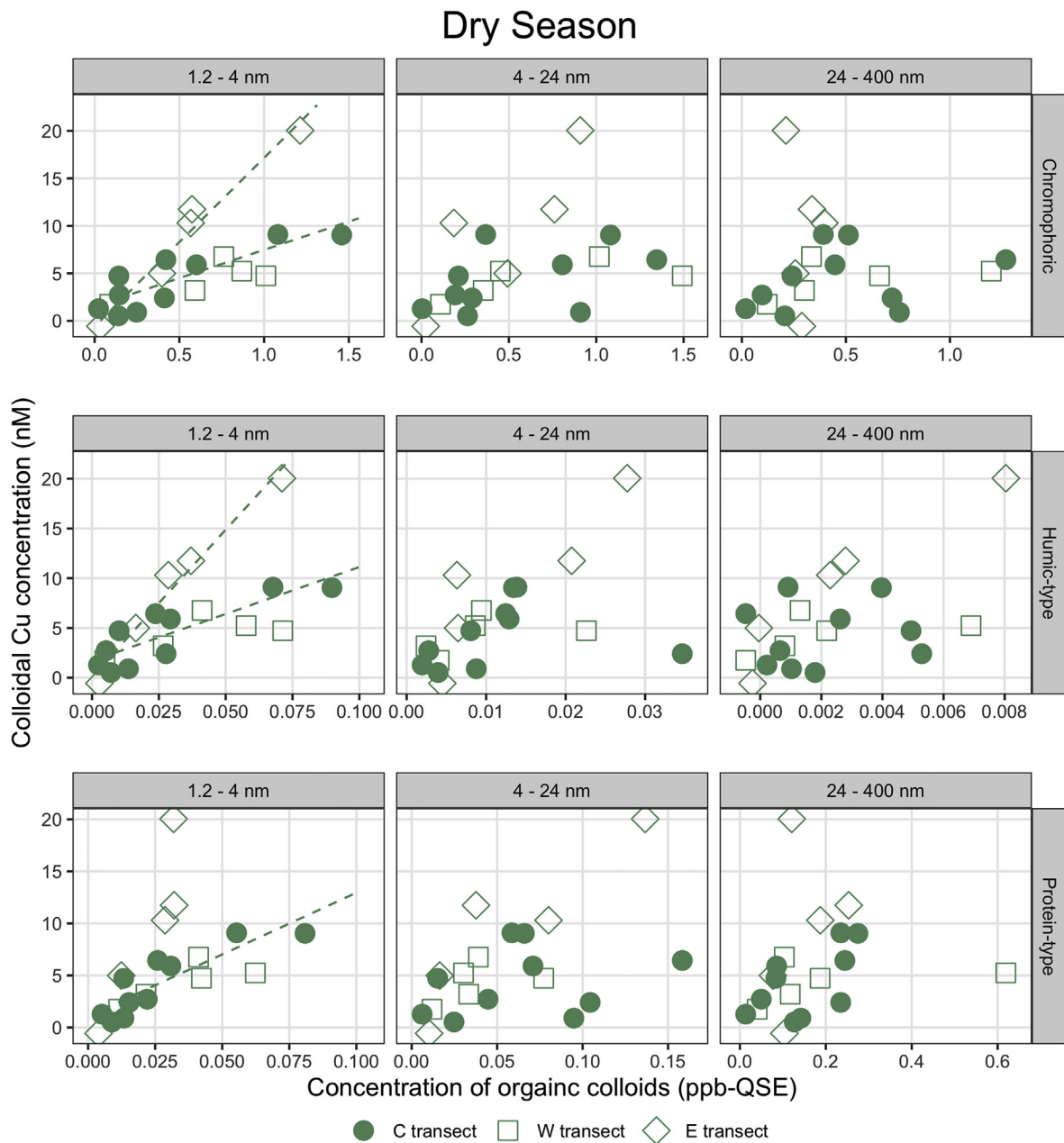


Fig. 8. Colloidal Cu was partitioned to organic colloids in the small size fraction. The concentration data of organic colloids was adapted from Xie et al. (2018). The dashed lines represent the linear fit for colloidal Cu and organic colloids ($p < 0.01$).

- Colloidal Cu showed high affinity for small-size organic colloids (likely fulvic acid) during the dry season. But the association between Cu and organic colloids during wet season was complex.

Declaration of competing interest

The authors declare that they have no known competing financial interests or personal relationships that could have appeared to influence the work reported in this paper.

CRedit authorship contribution statement

Minwei Xie: Conceptualization, Formal analysis, Writing -

original draft. **Wen-Xiong Wang:** Conceptualization, Formal analysis, Writing - original draft.

Acknowledgement

We thank Dr. Nanyan Weng, Dr. Guangyuan Lu, and Yunlong Li for their assistance in the field. M.X. specially thanks Dr. Qiao-Guo Tan for teaching how to use the software R. Dr. Graeme E. Batley, Dr. Brad Angel and three anonymous reviewers were greatly acknowledged for their valuable comments to improve the manuscript. This study was supported by National Natural Science Foundation of China (Grant No. 21707113 and 21777134), and the Hong Kong Branch of Southern Marine Science and Engineering Guangdong Laboratory (Guangzhou) (SMSEGL20SC01), and the TUYF fund (19SC01).

Appendix A. Supplementary data

Supplementary data to this article can be found online at <https://doi.org/10.1016/j.envpol.2020.114955>.

References

- Bianchi, T.S., 2007. *Biogeochemistry of Estuaries*. Oxford University Press on Demand.
- Brigden, K., Labunska, I., Santillo, D., Johnston, P., 2009. Hazardous Chemical Pollution of the Pearl River.
- Callahan, J., Dai, M., Chen, R.F., Li, X., Lu, Z., Huang, W., 2004. Distribution of dissolved organic matter in the Pearl River estuary, China. *Mar. Chem.* 89, 211–224.
- Chan, C.Y., Wang, W.-X., 2019b. Biomarker responses in oysters *Crassostrea hongkongensis* in relation to metal contamination patterns in the Pearl River Estuary, southern China. *Environ. Pollut.* 251, 264–276.
- Chen, B., Liang, X., Xu, W., Huang, X., Li, X., 2012. The changes in trace metal contamination over the last decade in surface sediments of the Pearl River Estuary, South China. *Sci. Total Environ.* 439, 141–149.
- Chen, J.-C., Heinke, G.W., Jiang Zhou, M., 2004. The Pearl River estuary pollution project (PREPP). *Continent. Shelf Res.* 24, 1739–1744.
- Comans, R.N., van Dijk, C.P., 1988. Role of complexation processes in cadmium mobilization during estuarine mixing. *Nature* 336, 151.
- Dai, M., Wang, L., Guo, X., Zhai, W., Li, Q., He, B., Kao, S.-J., 2008. Nitrification and Inorganic Nitrogen Distribution in a Large Perturbed River/estuarine System: the Pearl River Estuary, China.
- Day Jr., J.W., Hall, C.A., Kemp, W.M., Yanez-Arancibia, A., 1989. *Estuarine Ecology*. John Wiley & Sons.
- Dupra, V., Smith, S., Marshall Crossland, J., Crossland, C., 2000. Estuarine systems of the South China Sea region: carbon, nitrogen and phosphorus fluxes. *LOICZ Rep. Stud.* 14, 156pp.
- Dyer, K., 1991. Circulation and mixing in stratified estuaries. *Mar. Chem.* 32, 111–120.
- Fang, Z.-q., Cheung, R., Wong, M.H., 2003. Heavy metals in oysters, mussels and clams collected from coastal sites along the Pearl River Delta, South China. *J. Environ. Sci.* 15, 9–24.
- Harrison, P.J., Yin, K., Lee, J., Gan, J., Liu, H., 2008. Physical–biological coupling in the Pearl River estuary. *Continent. Shelf Res.* 28, 1405–1415.
- Hatje, V., Apte, S., Hales, L., Birch, G., 2003. Dissolved trace metal distributions in port jackson estuary (sydney harbour), Australia. *Mar. Pollut. Bull.* 46, 719–730.
- He, B., Dai, M., Zhai, W., Wang, L., Wang, K., Chen, J., Lin, J., Han, A., Xu, Y., 2010. Distribution, degradation and dynamics of dissolved organic carbon and its major compound classes in the Pearl River estuary, China. *Mar. Chem.* 119, 52–64.
- Hu, J., Li, S., Geng, B., 2011. Modeling the mass flux budgets of water and suspended sediments for the river network and estuary in the Pearl River Delta, China. *J. Mar. Syst.* 88, 252–266.
- Ip, C., Li, X., Zhang, G., Farmer, J., Wai, O., Li, Y., 2004. Over one hundred years of trace metal fluxes in the sediments of the Pearl River Estuary, South China. *Environ. Pollut.* 132, 157–172.
- Kraepiel, A.M., Chiffoleau, J.-F., Martin, J.-M., Morel, F.M., 1997. Geochemistry of trace metals in the Gironde estuary. *Geochem. Cosmochim. Acta* 61, 1421–1436.
- Li, X., Wai, O.W., Li, Y., Coles, B.J., Ramsey, M.H., Thornton, I., 2000. Heavy metal distribution in sediment profiles of the Pearl River estuary, South China. *Appl. Geochem.* 15, 567–581.
- Ma, L., Wang, W., Xie, M.-W., Wang, W.-X., Evans, R.D., 2020. Using Zn Isotopic Signatures for Source Identification in a Contaminated Estuary of Southern China. *Environmental science & technology*.
- Meng, F., Huang, G., Yang, X., Li, Z., Li, J., Cao, J., Wang, Z., Sun, L., 2013. Identifying the sources and fate of anthropogenically impacted dissolved organic matter (DOM) in urbanized rivers. *Water Res.* 47, 5027.
- Qian, W., Gan, J., Liu, J., He, B., Lu, Z., Guo, X., Wang, D., Guo, L., Huang, T., Dai, M., 2018. Current status of emerging hypoxia in a eutrophic estuary: the lower reach of the Pearl River Estuary, China. *Estuarine, Coastal and Shelf Science* 205, 58–67.
- Sohrin, Y., Urushihara, S., Nakatsuka, S., Kono, T., Higo, E., Minami, T., Norisuye, K., Umetani, S., 2008. Multielemental determination of GEOTRACES key trace metals in seawater by ICPMS after preconcentration using an ethylenediaminetriacetic acid chelating resin. *Anal. Chem.* 80, 6267–6273.
- Stolpe, B., Guo, L., Shiller, A.M., Hassellöf, M., 2010. Size and composition of colloidal organic matter and trace elements in the Mississippi River, Pearl River and the northern Gulf of Mexico, as characterized by flow field-flow fractionation. *Mar. Chem.* 118, 119–128.
- Stumm, W., Morgan, J.J., 2012. *Aquatic Chemistry: Chemical Equilibria and Rates in Natural Waters*. John Wiley & Sons.
- Tan, Q.-G., Lu, S., Chen, R., Peng, J., 2019. Making acute tests more ecologically relevant: cadmium bioaccumulation and toxicity in an estuarine clam under various salinities modeled in a toxicokinetic–toxicodynamic framework. *Environ. Sci. Technol.* 53, 2873–2880.
- van den Berg, C.M., Merks, A.G., Duursma, E.K., 1987. Organic complexation and its control of the dissolved concentrations of copper and zinc in the Scheldt estuary. *Estuar. Coast Shelf Sci.* 24, 785–797.
- Wang, D., Lin, W., Yang, X., Zhai, W., Dai, M., Chen, C.-T.A., 2012. Occurrences of dissolved trace metals (Cu, Cd, and Mn) in the Pearl River Estuary (China), a large river-groundwater-estuary system. *Continent. Shelf Res.* 50, 54–63.
- Wang, W., Chen, M., Guo, L., Wang, W.-X., 2017. Size partitioning and mixing behavior of trace metals and dissolved organic matter in a South China estuary. *Sci. Total Environ.* 603–604, 434–444.
- Wang, W.-X., Pan, K., Tan, Q., Guo, L., Simpson, S.L., 2014. Estuarine pollution of metals in China: science and mitigation. *Environ. Sci. Technol.* 48, 9975–9976.
- Weng, N., Wang, W.-X., 2019. Seasonal fluctuations of metal bioaccumulation and reproductive health of local oyster populations in a large contaminated estuary. *Environ. Pollut.* 250, 175–185.
- Wong, L., Chen, J., Xue, H., Dong, L., Guan, W., Su, J., 2003. A model study of the circulation in the Pearl River Estuary (PRE) and its adjacent coastal waters: 2. Sensitivity experiments. *J. Geophys. Res.: Oceans* 108.
- Xia, X., Li, Y., Yang, H., Wu, C., Sing, T., Pong, H., 2004. Observations on the size and settling velocity distributions of suspended sediment in the Pearl River Estuary, China. *Continent. Shelf Res.* 24, 1809–1826.
- Xie, M., Chen, M., Wang, W.-X., 2018. Spatial and temporal variations of bulk and colloidal dissolved organic matter in a large anthropogenically perturbed estuary. *Environ. Pollut.* 243, 1528–1538.
- Xie, M., Simpson, S.L., Wang, W.-X., 2019. Bioturbation effects on metal release from contaminated sediments are metal-dependent. *Environ. Pollut.* 250, 87–96.
- Xu, H., Zhong, J., Yu, G., Wu, J., Jiang, H., Yang, L., 2014. Further insights into metal-DOM interaction: consideration of both fluorescent and non-fluorescent substances. *PLoS One* 9, e112272.
- Yang, M., Sañudo-Wilhelmy, S.A., 1998. Cadmium and manganese distributions in the Hudson River estuary: interannual and seasonal variability. *Earth Planet Sci. Lett.* 160, 403–418.
- Yin, Q., Wang, W.-X., 2017. Relating metals with major cations in oyster *Crassostrea hongkongensis*: a novel approach to calibrate metals against salinity. *Sci. Total Environ.* 577, 299–307.
- Yu, X.-J., Pan, K., Liu, F., Yan, Y., Wang, W.-X., 2013. Spatial variation and subcellular binding of metals in oysters from a large estuary in China. *Mar. Pollut. Bull.* 70, 274–280.
- Zhang, G., Cheng, W., Chen, L., Zhang, H., Gong, W., 2019. Transport of riverine sediment from different outlets in the Pearl River Estuary during the wet season. *Mar. Geol.* 415, 105957.

Supporting Information for

**Contrasting temporal dynamics of dissolved and colloidal trace metals in
the Pearl River Estuary**

Minwei Xie^{1,2}, Wen-Xiong Wang^{2,3*}

¹ *College of the Environment and Ecology, Xiamen University, Fujian 361102, China*

² *Research Centre for the Oceans and Human Health, City University of Hong Kong
Shenzhen Research Institute, Shenzhen 518057, China*

³ *School of Energy and Environment, State Key Laboratory of Marine Pollution, City
University of Hong Kong, Kowloon, Hong Kong, PR China*

* Corresponding author, wx.wang@cityu.edu.hk

S1. Quality control results

The preconcentration of water samples using Nobias chelate PA-1 resin induce minimal contamination of water samples (Table S2, Supporting Information). Metal concentrations in the procedural blank samples were below instrumental detection limit for Ni, Cu, and Zn and approximated detection limit for manganese and cadmium (Table S2). The relative standard deviations (RSDs) in the metal–spiked seawater samples, which were processed concurrently with estuarine water samples during the preconcentration procedure, were uniformly low (<10%) for all metals, indicating high consistency and reproducibility of the preconcentration method. The recoveries using certified reference material (NASS-6 and SLEW-3) were between 90-115%, validating the accuracy of the preconcentration method.

S2. Assessing the remobilization of Cd along the C-transect during the wet season

Distribution of total dissolved Cd along C-transect was different from that of other metals, such as Cu, Ni, and Zn in the wet season. Instead of decreasing in concentrations with increasing salinity, total dissolved Cd concentration increased over the low salinity region (salinity < 7) but slightly decrease in the higher salinity region (salinity >12). It has been well documented that desorption of Cd occurred during estuarine mixing when salinity increased (Comans and van Dijk, 1988; Yang and Sañudo-Wilhelmy, 1998). To assess the contribution of desorption induced cadmium mobilization, particulate Cd (> 0.4 μm) concentrations were quantified using microwave facilitated digestion with 10 mL concentrated nitric acid following the USEPA method 3051A. As shown in Figure S3a, increase in dissolved Cd concentrations and decrease in particulate Cd concentrations occurred concurrently, suggesting that desorption was involved in the remobilization of cadmium. Therefore, to explore the contribution of desorption process to the net remobilization of cadmium along the C-transect, we calculated the net gains or losses of cadmium by comparing the difference between measured and theoretical concentrations of cadmium in the total dissolved and particulate fraction (El Sayed et al., 1994; Yang and Sañudo-Wilhelmy, 1998).

The calculation needs to meet the following assumptions: 1) conservative behavior of suspended particulate matter during the estuarine mixing; 2) homogeneous distribution of metal in the particulate fraction (El Sayed et al., 1994). These assumptions hold for the present study as Cd has higher affinity for finer particles, which were prone to suspension considering the hydrology of the PRE during the wet season, with a short water residence time and strong flow hydrodynamics.

Accordingly, we calculated theoretical concentrations (assuming conservative mixing) of Cd in the total dissolved and particulate fraction using the Cd concentrations in two endmembers with the lowest and highest salinity (Figure S3a, indicated as the dashed lines). The net gains or losses of Cd in each pool was calculated as the difference between the measured and the extrapolated Cd concentrations (Figure S3b). The resulting positive and negative values indicated gains and losses in each pool respectively. Considering data variability, the net gains and losses of Cd calculated were not compared directly, but each fitted using a quadratic polynomial model. The simulated gains and losses values were then calculated at each measured salinity, and the ratio of losses to gains were then calculated.

As the free Cd^{2+} activity in the solution regulates the desorption of Cd (Comans and van Dijk, 1988), we also calculated the free Cd^{2+} activity in the estuarine water using the ChemEQL (v2.0) software (Müller, 1996). Reactions of Cd species involved and stability constants were listed in Table S4. The pH at each site was from Table S1. Except a few sites (HuMen, C1 and C5), the free Cd^{2+} activity was strongly correlated with particulate Cd concentrations, following a linear sorption isotherm model (Figure S3c), suggesting that equilibrium was reached at most sites along the C-transect within the water residence time, and more importantly, the desorption of Cd was regulated by decreasing Cd^{2+} activity along the salinity gradient.

S3. Distribution of truly dissolved metals along the estuary

Distribution of metal concentrations in the truly dissolved fraction (< 1kDa) is shown in Figures S6 and S7. Concentrations of these metals were of similar magnitudes as the total dissolved metals. Overall, the spatial distribution of truly dissolved metal concentrations was also similar to the total dissolved fraction. During the dry season, concentrations of all metals declined along the C-transect. In the middle estuary reach, metal concentrations in the W- and E- transects were lower and higher relative to the corresponding sites at the C-transect. The distributions of metal concentrations were consistent among the three transects in the lower estuary reach. During the wet season, Mn and Cd concentrations also increased seaward in the lower salinity region (salinity <7) but slightly decreased when the salinity exceeded 12 (Figure S7). Cu concentrations rapidly declined along the C-transect and approached to a constant level (Figure S7). Ni and Zn concentrations did not exhibit any evident patterns but varied at $0.59 \pm 0.21 \mu\text{g/L}$ and $0.046 \pm 0.024 \mu\text{g/L}$, respectively.

Dry Season

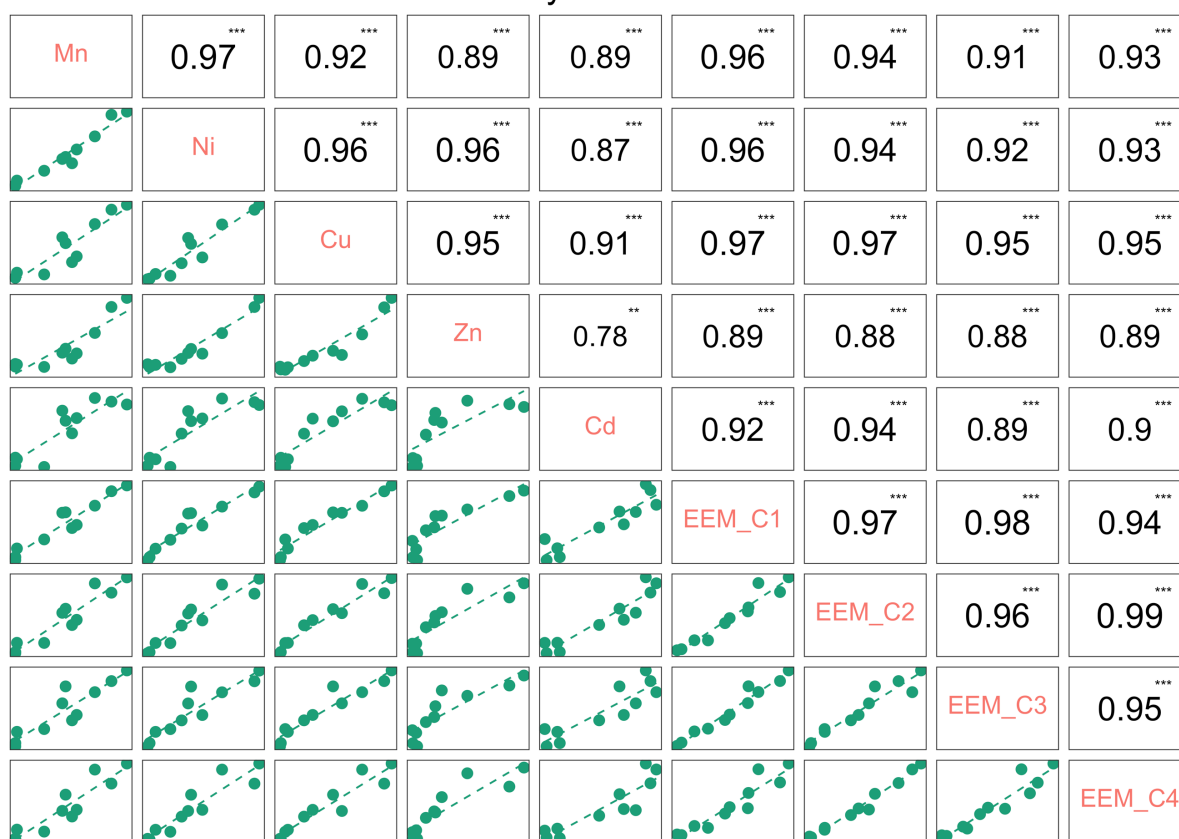


Figure S1. The pairwise correlation between metal concentrations and fluorescence intensity of DOM components (EEMs_C1 to _C4) along the C-transect during the dry season. Lower triangle: scatter plots; upper triangle: Pearson correlation coefficients and level of significance (** $p < 0.01$, * $p < 0.05$, and the larger font size of the correlation coefficients indicates higher significant levels). Data for the fluorescent intensity of DOM components were adapted from Xie et al. (2018).

Wet Season

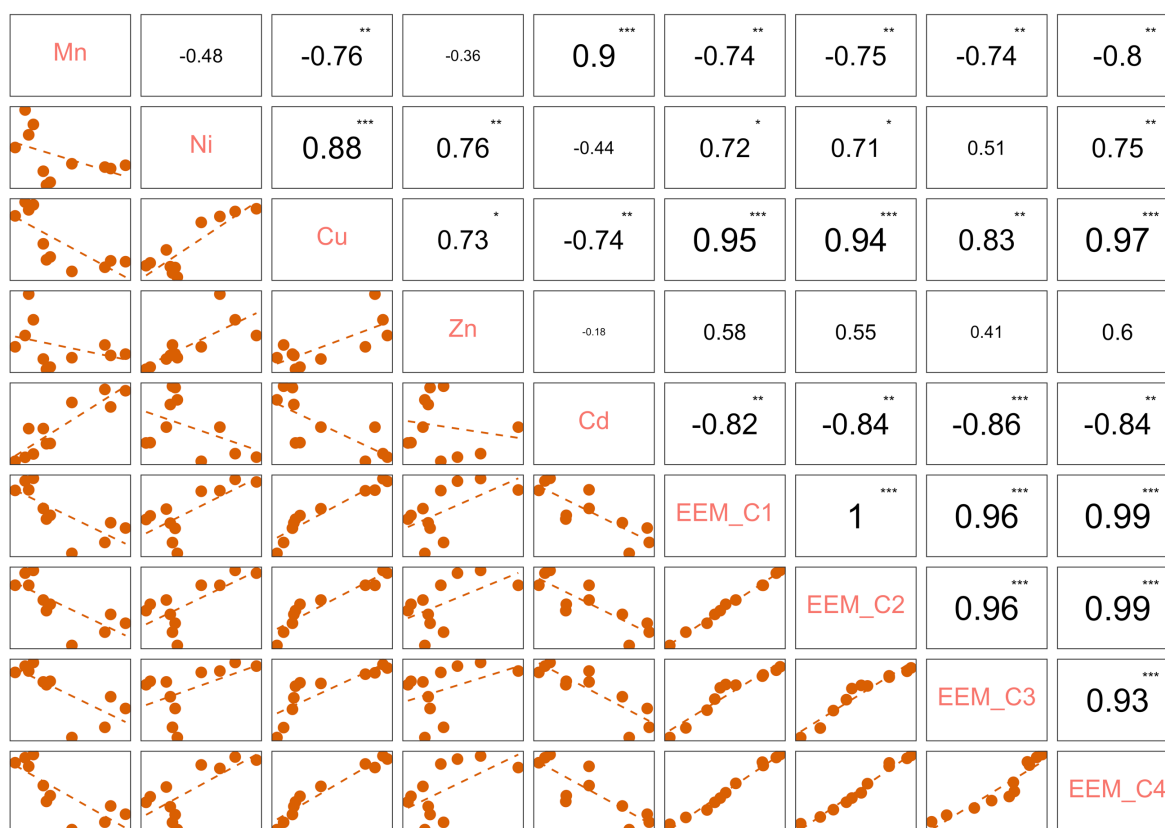


Figure S2. The pairwise correlation between metal concentrations and fluorescence intensity of DOM components (EEMs_C1 to _C4) along the C-transect during the wet season. Lower triangle: scatter plots; upper triangle: Pearson correlation coefficients and level of significance (** $p < 0.01$, * $p < 0.05$, and the larger font size of the correlation coefficients indicates higher significant levels). Data for the fluorescent intensity of DOM components were adapted from Xie et al. (2018).

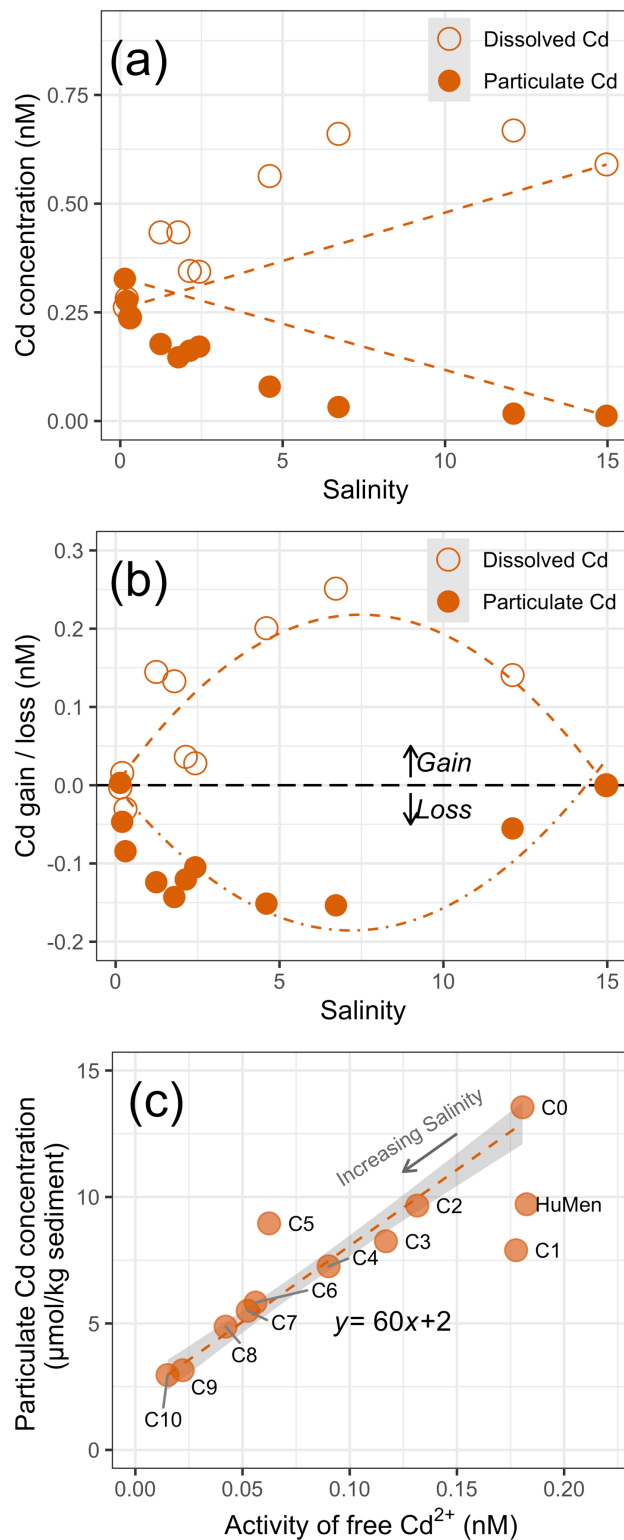


Figure S3. (a) Distribution of dissolved and particulate Cd along the C-transect during the wet season. The dashed lines represent theoretical conservative mixing lines for dissolved and particulate Cd respectively. (b) Net remobilization of Cd in the dissolved and particulate pool during the estuarine mixing. Positive values indicate gains and negative values represent losses. The horizontal dash line intercept at $y = 0$ indicates no loss or gain of Cd.

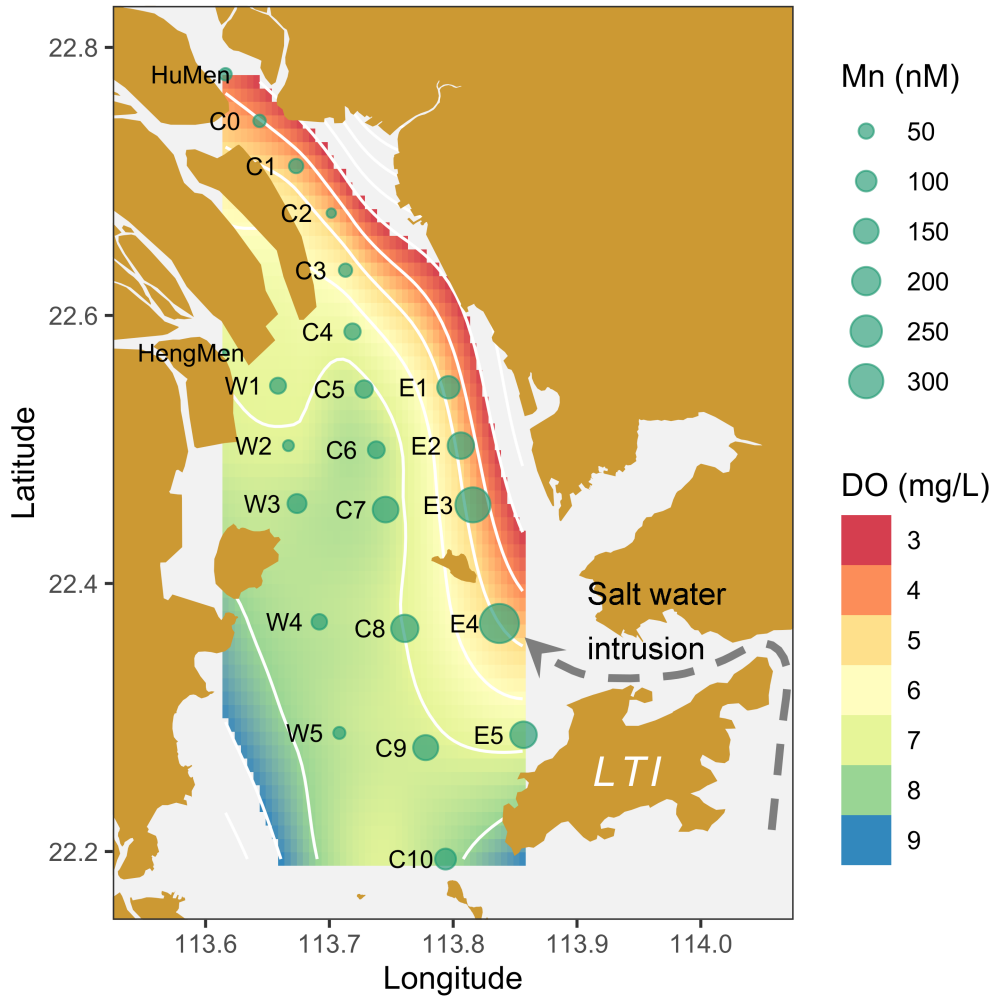


Figure S4. Contour of DO concentration and distribution of total dissolved Mn concentrations in the estuary during the wet season. The grey arrow around the Lantau island (LTI) indicates the saltwater intrusion path along the east channel during the wet season.

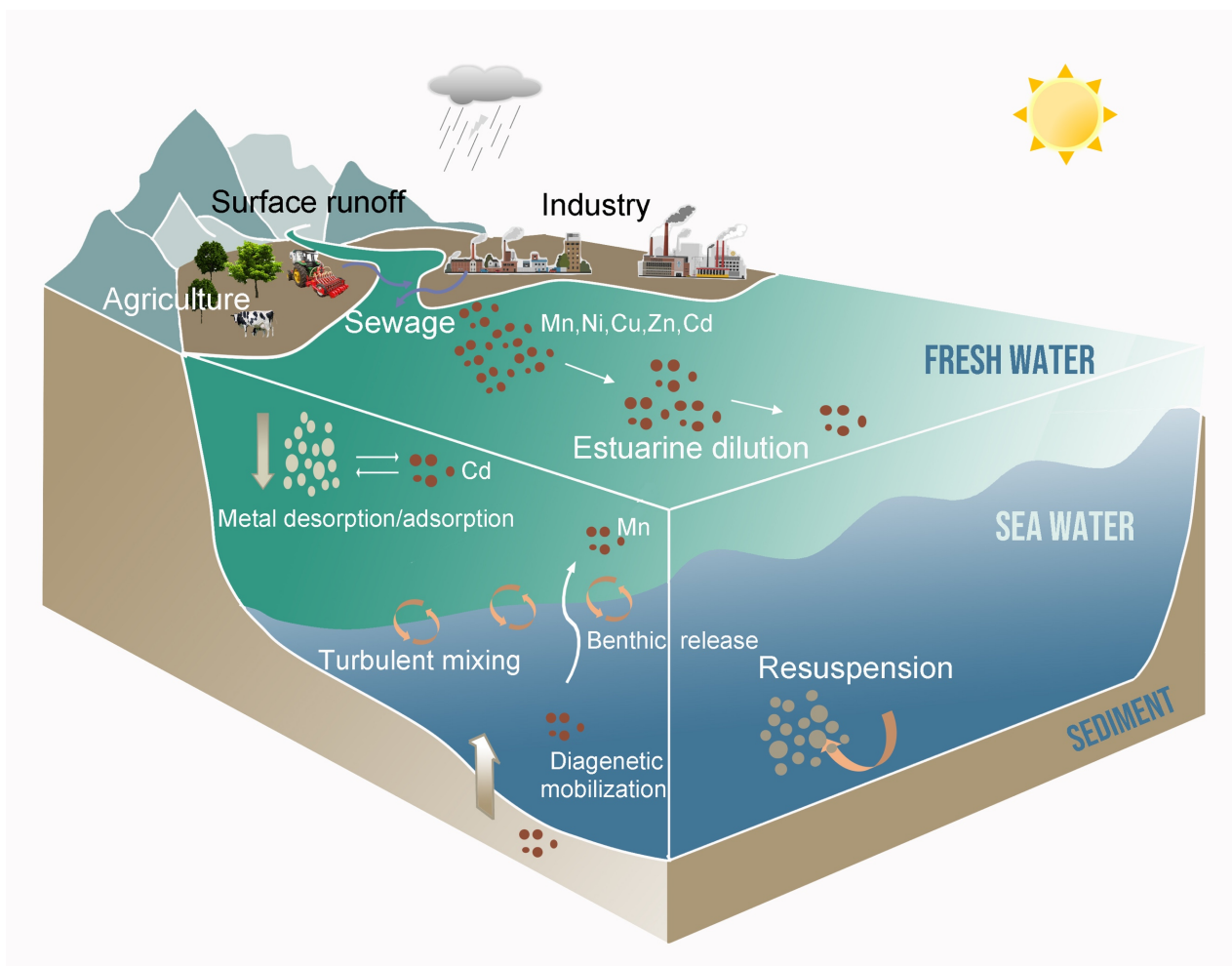


Figure S5. Processes affecting the fate of metals in the estuary.

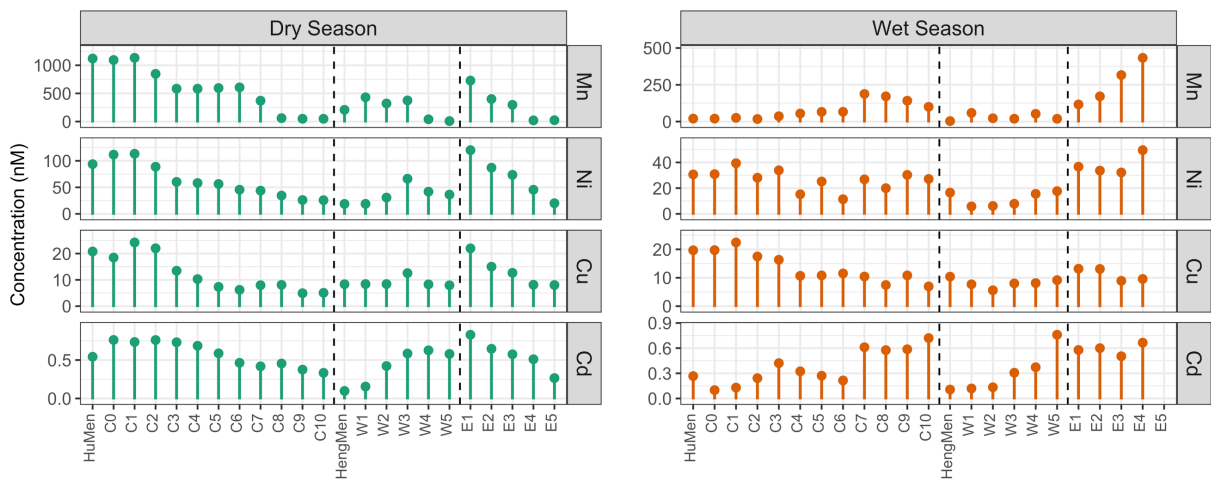


Figure S6. Truly dissolved metal concentrations in the surface water samples collected from the PRE during the dry and wet season. Metal concentrations at Site E5 during the wet season are not available due to leakage of water sample in the preconcentration step.

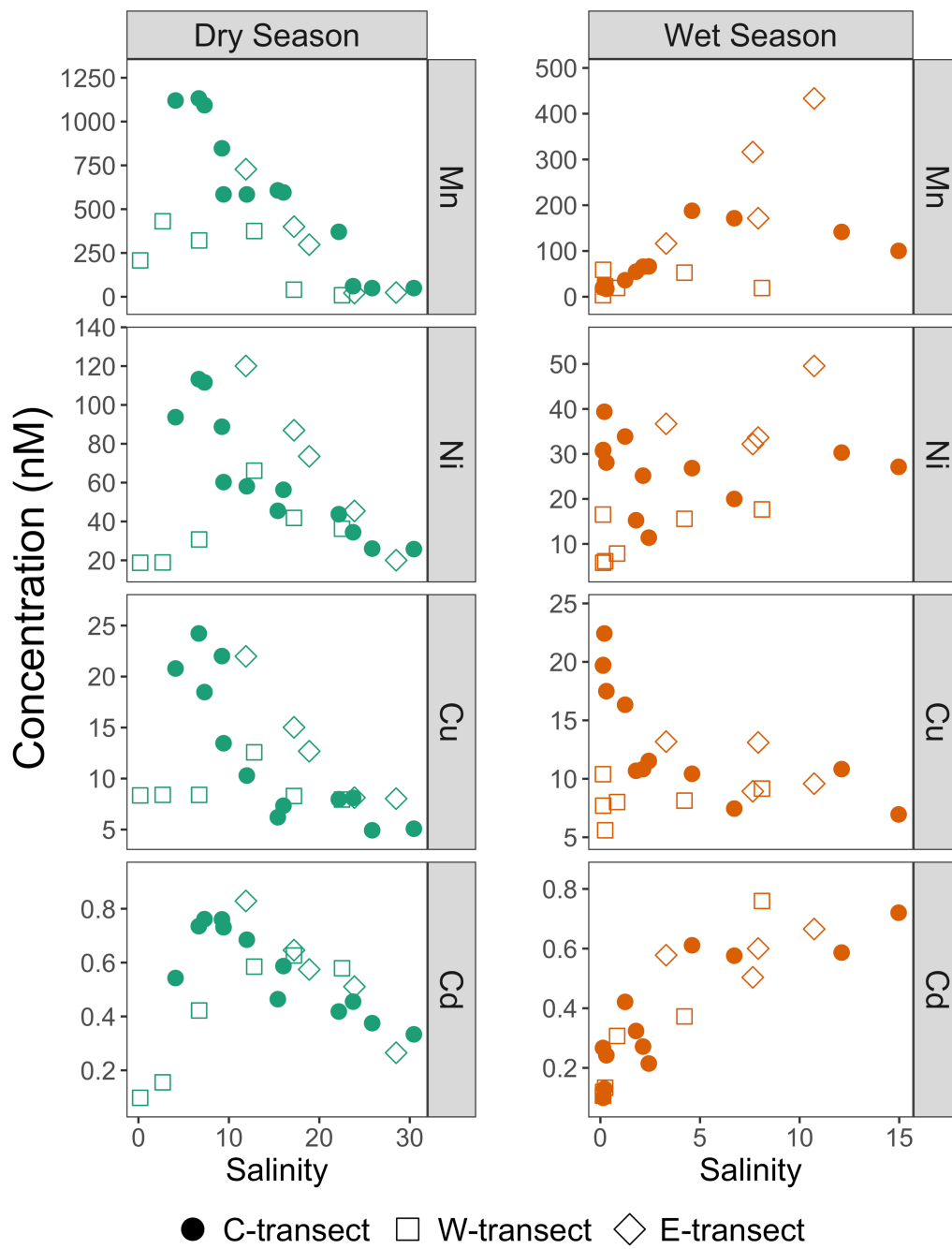


Figure S7. Distribution of truly dissolved metals along each transect during the dry and wet season.

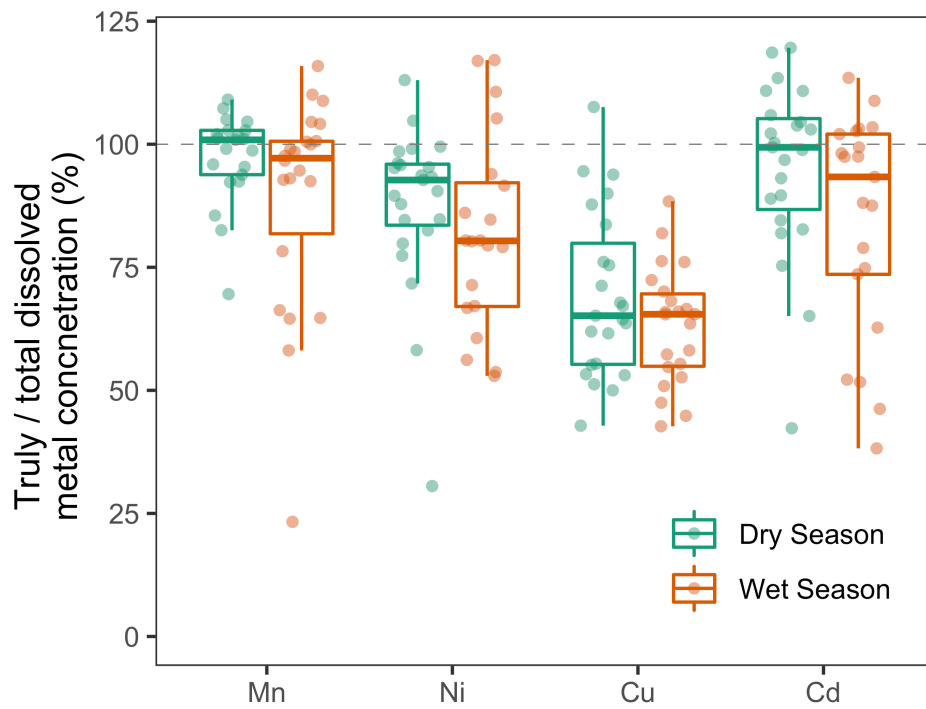


Figure S8. Percentage of truly dissolved metal concentrations to bulk dissolved metal concentrations in water samples collected along the PRE.

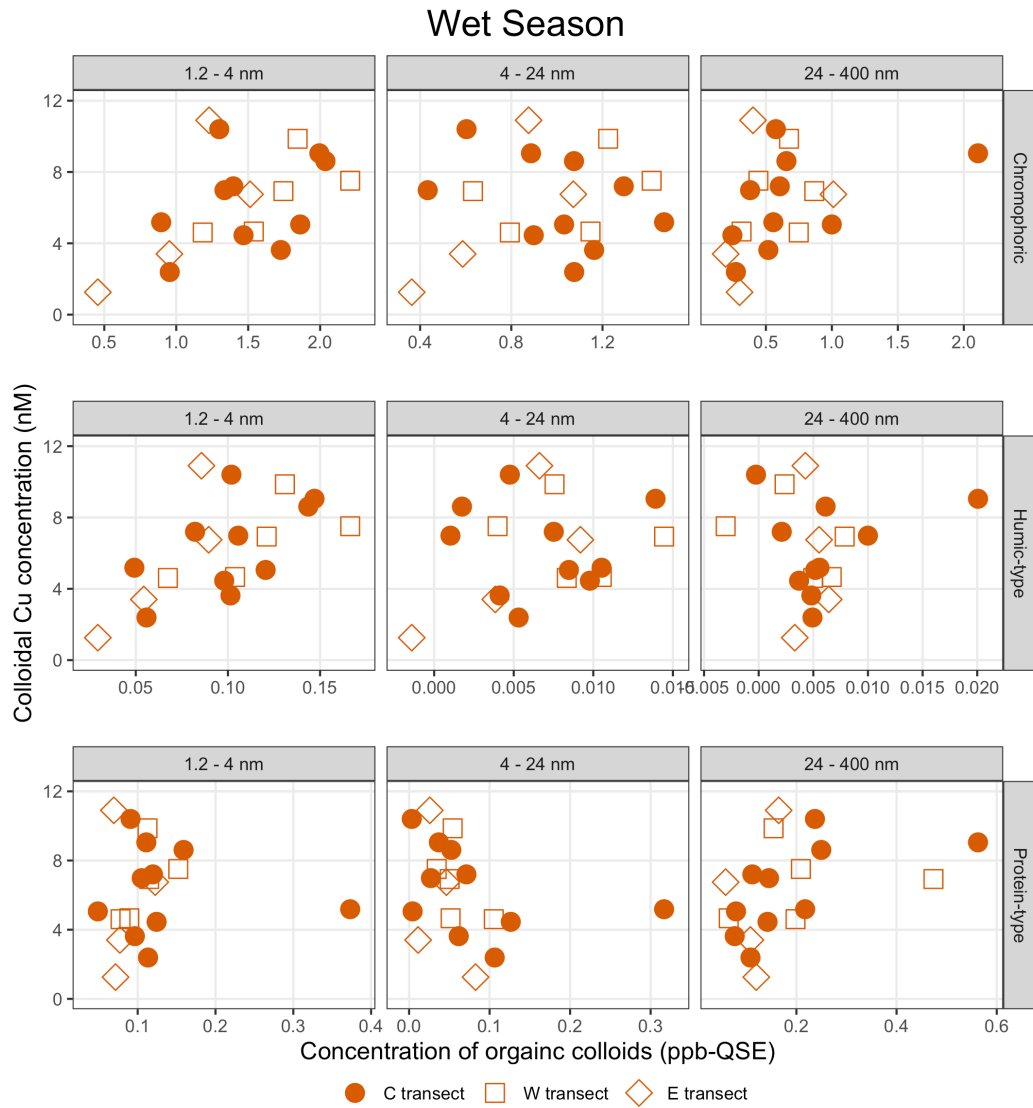


Figure S9. Correlations between colloidal Cu and organic colloids in different size fractions during the wet season.

Table S1. Physico-chemical parameters of water samples along the estuary

	Sites	Salinity ¹	Dissolved oxygen concentration (mg/L) and Saturation ² (%)	pH	
Dry Season	River outlets	HuMen	4.10	3.40 (38%)	8.04
		JiaoMen	0.22	6.77 (75%)	8.34
		HengMen	0.19	7.29 (80%)	8.39
	C-transect	C0	7.30	4.6 (53%)	7.61
		C1	6.67	4.13 (47%)	7.84
		C2	9.23	6.75 (79%)	7.87
		C3	9.41	6.72 (78%)	8.02
		C4	12.0	6.79 (80%)	7.91
		C5	16.0	6.71 (81%)	8.04
		C6	15.4	7.31 (88%)	7.89
		C7	22.2	6.64 (83%)	7.95
		C8	23.7	7.12 (90%)	7.91
		C9	25.8	7.52 (96%)	7.85
	C10	30.5	8.18 (108%)	7.91	
	W-transect	W1	2.68	7.30 (82%)	8.30
		W2	6.71	7.05 (81%)	8.06
		W3	12.8	7.05 (84%)	7.73
		W4	17.2	6.95 (85%)	7.91
		W5	22.5	7.37 (93%)	7.87
	E-transect	E1	11.9	8.42 (100%)	7.93
E2		17.2	7.39 (90%)	7.73	
E3		18.9	7.01 (86%)	7.85	
E4		23.9	7.95 (101%)	7.91	
E5		28.5	8.09 (106%)	8.02	
Wet Season	River outlets	HuMen	0.13	3.43 (46%)	6.66
		JiaoMen	0.13	6.37 (86%)	6.21
		HengMen	0.13	6.81 (91%)	8.08
	C-transect	C0	0.14	4.34 (58%)	7.63
		C1	0.20	4.32 (58%)	7.64
		C2	0.30	4.99 (67%)	7.86
		C3	1.24	5.28 (71%)	7.94
		C4	1.79	6.26 (85%)	8.06
		C5	2.14	8.57 (116%)	8.23
		C6	2.43	7.02 (95%)	8.24
		C7	4.60	7.10 (98%)	8.25
		C8	6.72	7.11 (99%)	8.22
		C9	12.1	7.17 (102%)	8.25
	C10	15.0	7.14 (104%)	8.27	
	W-transect	W1	0.14	7.05 (95%)	8.13
		W2	0.24	6.81 (92%)	8.19
		W3	0.84	6.88 (93%)	8.23
		W4	4.22	7.12 (98%)	8.23
		W5	8.11	7.52 (105%)	8.33
	E-transect	E1	3.30	4.79 (65%)	7.96
E2		7.92	4.68 (65%)	7.95	
E3		7.65	4.18 (58%)	8.09	
E4		10.7	3.49 (49%)	8.01	
E5		13.2	7.64 (110%)	8.17	

¹ The salinity data are adopted from (Xie et al., 2018).

² Saturation was calculated by dividing DO concentrations to oxygen solubility. Oxygen solubility at each salinity was linearly interpolated based on the oxygen solubility table (<https://www.ysi.com/parameters/dissolved-oxygen>). The temperature during the sample collection was $20.2 \pm 0.6^\circ\text{C}$ and $30.7 \pm 0.4^\circ\text{C}$ for the dry season and wet season, respectively.

Table S2. Blanks, detection limits and recovery of operational and analytical procedures.

	Preconcentration procedure		Filtration	Ultrafiltration	Mean concentrations (RSD%) in spiked seawater samples ³			Column	Instrument
	Instrument detection limit (µg/L)	Procedural blank (µg/L)	Blank ¹ (µg/L)	Blank ² (µg/L)	Batch 1 n = 10	Batch 2 n = 12	NASS6 n=2	SLEW3 n=1	SLRS6 n=5
Mn	0.012	0.013	0.032	0.032	4.03 (8.9%)	1.98 (4.5%)	91%	90%	92%
Ni	0.019	BDL	BDL	BDL	4.20 (10%)	2.77 (4.7%)	98%	107%	88%
Cu	0.074	BDL	BDL	BDL	2.71 (4.1%)	2.47 (4.4%)	102%	95%	96%
Zn	0.105	BDL	0.126	1.24	7.94 (8.9%)	4.20 (9.5%)	97%	107%	99%
Cd	0.002	0.006	0.005	0.008	2.14 (7.0%)	2.00 (5.0%)	100%	115%	113%

BDL means below detection limit

^{1,2} Filtration/ultrafiltration blank samples were subject to both the filtration/ultrafiltration and preconcentration procedures.

³ Representing the concentration sum of spiked metals and metals originally present in the seawater. Low RSD indicated high reproducibility of the preconcentration operations.

Table S3. Total dissolved metal concentration in the river outlets during the dry and wet season.

		Metal concentrations ($\mu\text{g/L}$)										Colloidal fraction (%)									
		Total dissolved (< 0.4 μm)					Truly dissolved (< 1 kDa)														
		Mn	Ni	Cu	Zn	Cd	Mn	Ni	Cu	Zn	Cd	Mn	Ni	Cu	Zn	Cd	Mn	Ni	Cu	Zn	Cd
Dry Season	HuMen	62.3	6.5	1.75	3.27	0.081	61.5	5.5	1.32	3.2	0.061	1	16	25	2	25					
	JiaoMen	8.45	3.7	3.40	7.19	0.045	6.47	2.6	1.60	3.5	0.034	23	30	53	52	24					
	HengMen	10.9	3.6	1.06	0.37	0.026	11.4	1.1	0.53	0	0.011	–	68	50	–	58					
Wet Season	HuMen	1.70	3.4	1.91	0.77	0.029	1.1	1.8	1.25	0.54	0.03	35	46	35	30	0					
	JiaoMen	0.53	1.0	1.83	0.68	0.024	0.42	0.46	0.72	0.25	0.020	21	56	61	63	17					
	HengMen	0.23	1.6	1.39	0.25	0.023	0.18	0.97	0.66	0.37	0.012	22	38	53	–	48					

Table S4. Reactions and stability constants used in the Cd speciation model.

Reaction	Log(K)
$\text{Cd}^{2+} = \text{Cd}^{2+}$	
$\text{Cd}^{2+} + \text{OH}^- = \text{Cd}(\text{OH})^+$	-10.1
$\text{Cd}^{2+} + 2\text{OH}^- = \text{Cd}(\text{OH})_2$	-20.4
$\text{Cd}^{2+} + 3\text{OH}^- = \text{Cd}(\text{OH})_3^-$	-33.3
$\text{Cd}^{2+} + 4\text{OH}^- = \text{Cd}(\text{OH})_4^{2-}$	-47.4
$\text{Cd}^{2+} + \text{Cl}^- = \text{CdCl}^+$	2.0
$\text{Cd}^{2+} + 2\text{Cl}^- = \text{CdCl}_2$	2.6
$\text{Cd}^{2+} + 3\text{Cl}^- = \text{CdCl}_3^-$	2.4
$\text{Cd}^{2+} + 4\text{Cl}^- = \text{CdCl}_4^{2-}$	1.7

†Activity coefficients were calculated with the Davies equation (Stumm and Morgan, 2012).

Table S5. Pearson coefficient and significance levels between concentrations of colloidal Cu and chromophoric organic colloids based on partial correlation analysis.

		Colloidal size fractions		
		1.2–4 nm	4–24 nm	24–400 nm
Dry Season	C-transect	0.845**	0.505	0.478
	W-transect	0.830	0.791	0.236
	E-transect	0.994**	0.586	-0.659
Wet Season	C-transect	-0.118	-0.023	0.325
	W-transect	0.042	0.240	0.314
	E-transect	0.662	0.805	0.911

** p < 0.01

Table S6. Pearson coefficient between concentrations of colloidal Cu and humic-type organic colloids.

		Colloidal size fractions		
		1.2–4 nm	4–24 nm	24–400 nm
Dry Season	C-transect	0.826**	0.555	0.115
	W-transect	0.693	0.505	0.224
	E-transect	0.983**	0.719	0.957
Wet Season	C-transect	0.181	0.152	0.066
	W-transect	0.013	-0.414	-0.339
	E-transect	0.793	0.644	-0.262

** p < 0.01

Table S7. Pearson coefficient between concentrations of colloidal Cu and protein-type organic colloids.

		Colloidal size fractions		
		1.2–4 nm	4–24 nm	24–400 nm
Dry Season	C-transect	0.847**	0.603	0.743*
	W-transect	0.667	0.735	0.047
	E-transect	0.798	0.952*	-0.768
Wet Season	C-transect	0.556	0.226	0.595
	W-transect	-0.037	0.563	-0.258
	E-transect	0.740	0.606	-0.528

** p < 0.01 * p < 0.05

Reference:

Comans, R.N., van Dijk, C.P., 1988. Role of complexation processes in cadmium mobilization during estuarine mixing. *Nature* 336, 151.

El Sayed, M.A., Aminot, A., Kerouel, R., 1994. Nutrients and trace metals in the northwestern Mediterranean under coastal upwelling conditions. *Continental Shelf Research* 14, 507-530.

Müller, B., 1996. ChemEQL: a program to calculate chemical speciation equilibria titrations, dissolutions, precipitation, adsorption, simple kinetics, and pX-pY diagrams. Swiss Federal Institute for Environmental Science and Technology (EAWAG), Kastanienbaum, Switzerland.

Stumm, W., Morgan, J.J., 2012. *Aquatic chemistry: chemical equilibria and rates in natural waters*. John Wiley & Sons.

Xie, M., Chen, M., Wang, W.-X., 2018. Spatial and temporal variations of bulk and colloidal dissolved organic matter in a large anthropogenically perturbed estuary. *Environmental pollution* 243, 1528-1538.

Yang, M., Sañudo-Wilhelmy, S.A., 1998. Cadmium and manganese distributions in the Hudson River estuary: interannual and seasonal variability. *Earth and Planetary Science Letters* 160, 403-418.